Signaling protein abundance modulates the strength of the Spindle Assembly Checkpoint

Chu Chen[1,2,3,*], Lauren Humphrey[1,*], Soubhagyalaxmi Jema[1], Shriya Karmarkar[1], Frank Ferrari[1], Ajit P. Joglekar[1,2]

1 - Department of Cell and Developmental Biology, University of Michigan Medical School, Ann Arbor, Michigan 48109

2 - Department of Biophysics, University of Michigan, Ann Arbor, Michigan 48109

3 – current address: Department of Molecular Genetics of Ageing, Max Planck Institute for Biology of Ageing, Cologne, Germany 50931

* - equal contribution

Corresponding author: ajitj@umich.edu

Summary

During mitosis, unattached kinetochores in a dividing cell signal to the Spindle Assembly Checkpoint to delay anaphase onset and prevent chromosome missegregation [1-4]. The signaling activity of these kinetochores and the likelihood of chromosome missegregation both depend on the amount of SAC signaling proteins that each kinetochore recruits [5-8]. Therefore, factors that control SAC protein recruitment to signaling kinetochores must be thoroughly understood. Phosphoregulation of kinetochore and SAC signaling proteins emerging from the concerted action of many kinases and phosphatases is a major determinant of SAC protein recruitment to signaling kinetochores [9]. Whether the abundance of SAC proteins also influences their recruitment and signaling activity at human kinetochores has not been studied [8,10]. Here, we reveal that the low cellular abundance of the SAC signaling protein Bub1 limits kinetochore recruitment of Bub1 and BubR1 and reduces the SAC signaling activity of the kinetochore. Conversely, Bub1 overexpression results in higher protein recruitment and SAC activity producing longer delays in anaphase onset. We also find that the number of SAC proteins recruited by a signaling kinetochore is inversely correlated with the total number of signaling kinetochores in the cell. This correlation likely arises from the competition among the signaling kinetochores to recruit from a limited pool of signaling proteins. The inverse correlation between the number of signaling kinetochores in the cell and the signaling activity of individual kinetochores may allow the dividing cell to prevent the large number of signaling kinetochores in prophase from generating an unnecessarily large signal, while enabling the last unaligned kinetochore to signal at the maximum possible strength.

Results and Discussion

The stoichiometry of SAC proteins at signaling kinetochores depends on the number of signaling kinetochores in the cell

We set two interrelated goals for this study. First, we wanted quantify the steady-state stoichiometry of key SAC proteins in human kinetochores to directly view the signaling activity of individual kinetochores [6]. This has been accomplished in fungi [8,10], but the data in vertebrates remains indirect and fragmentary [5,11]. Therefore, we quantified the recruitment of three SAC proteins representing the three layers of the well-defined signaling cascade that generates the 'Mitotic Checkpoint Complex' (MCC, Figure 1A) [5,12-21]. To accomplish this, we used three genome-edited HeLa-A12 cell lines wherein either Bub1, BubR1, or Mad1 was fused with mNeonGreen (mNG) [22,23]. These HeLa cell lines are only partially genome-edited; fully edited cell lines could not be obtained because of low efficiency of CRISPR-Cas9-mediated knock-ins and the pseudo-tetraploid nature of HeLa cells. Therefore, we also quantified the relative amounts of labeled and unlabeled proteins in the three cell lines using quantitative immunoblot analysis on whole-cell lysates of mitotic cells (Figure S1A-B). This analysis defined the labeled-to-unlabeled protein ratio for each of the three cell lines: ~40% for Bub1 and ~70% for both BubR1 and Mad1 (assuming similar transfer efficiencies for the labeled and unlabeled protein bands, Figure S1C). We used these ratios to estimate the total protein recruitment per kinetochore from the average signal for the mNG-tagged protein per kinetochore. It should be noted that these fusions do not detectably affect SAC signaling (shown later in Figure 4).

For our second goal, we studied whether the number of signaling kinetochores in the cell affects the signaling activity of individual kinetochores. In budding yeast, the recruitment of SAC proteins per kinetochore is higher in cells that contain fewer signaling kinetochores, likely because of the limited abundance of SAC proteins [10]. Whether this factor influences the signaling activity of human kinetochores is unknown. Therefore, we observed SAC protein recruitment per kinetochore in mitotically arrested cells containing two distinctly different numbers of signaling kinetochores. To obtain cells with nearly all kinetochores signaling, we released G1/S arrested HeLa cells into the cell cycle and then arrested them in mitosis using 330 nM nocodazole to depolymerize microtubules (Figure 1B, right). These cells serve as a model for late prophase. To obtain mitotic cells with a much smaller number of signaling kinetochores, we released G1/S arrested HeLa cells into the cell cycle and treated them with 236 nM GSK923295, a small molecule inhibitor of the mitotic kinesin CENP-E, 1.5 hours prior to imaging [24]. These cells model late prometaphase, because most of the chromosomes align at the metaphase plate, but a

65 smaller, variable number of chromosomes become stranded at the spindle poles. The unattached
66 or laterally attached kinetochores of these chromosomes activate the SAC (Figure 1B, left) [25,26].
67 Relying on visual inspection, we selected only those cells containing ~ 10 or less polar
68 chromosomes for analysis.

69 The quantitative comparison of mNG-labeled protein recruitment revealed that the recruitment of
70 all three proteins per kinetochore was significantly higher in GSK923295-treated compared to
71 nocodazole-treated cells (Figure 1C). We combined these measurements with the quantitative
72 immunoblotting data to estimate the total (labeled + unlabeled) protein amount to understand how
73 BubR1 and Mad1 recruitment correlates with Bub1 recruitment after the two treatments (Figure
74 1D). We normalized total protein amounts with the amount of total Bub1 per kinetochore in
75 GSK923295-treated cells [13,27-32]. In GSK923295-treated cells, BubR1 and Mad1 per kinetochore
76 was ~ 60 and 45% respectively of total Bub1 per kinetochore. In nocodazole-treated cells, the
77 BubR1 and Mad1 amount per kinetochore was significantly lower ~ 40% and 25% respectively of
78 total Bub1. Thus, the overall protein recruitment per kinetochore was higher in GSK923295-
79 treated cells compared to nocodazole-treated cells: 1.45-fold in case of Bub1, 2.3-fold and 2.6-
80 fold for BubR1 and Mad1 respectively (Figure 1D). Thus, the number of SAC proteins recruited
81 per kinetochore in HeLa cells is inversely correlated with the number of signaling kinetochores in
82 the cell, consistent with observations in budding yeast [10].

83 We used a fluorescence standard to estimate the copy number of each SAC protein recruited per
84 kinetochore. It is known that: (a) the human kinetochore contains ~ 250 molecules of the Ndc80
85 complex and (b) the stoichiometry between Ndc80 and Knl1 is 3:2 [33]. Therefore, under identical
86 imaging conditions we imaged HeLa cells exogenously overexpressing Spc25-mNG (Spc25 is an
87 Ndc80 complex subunit) and treated with siRNA targeting the endogenous Spc25 to quantify the
88 mNG signal per kinetochore in metaphase cells (Figure S1D). Using the above-mentioned
89 parameters, we converted the estimated total amount of each protein per kinetochore into the
90 number of molecules of the protein recruited per Knl1 molecule in HeLa cells. These calculations
91 indicate that each Knl1 molecule recruits 5 ± 0.9 Bub1 molecules, 3 ± 0.7 BubR1 molecules, and
92 2 ± 0.7 Mad1 molecules in GSK923295-treated cells. The numbers are lower in nocodazole-
93 treated cells: 3 ± 0.7 Bub1 molecules, and 1 ± 0.4 molecules of BubR1 and Mad1 each per Knl1.
94 The number of Bub1 molecules per kinetochore in nocodazole-treated cells is slightly lower than
95 the previously reported number of 4-6 molecules [5,12,13]. A more recent study found that Bub1
96 recruitment per kinetochore was not significantly different in cells treated with nocodazole- and

97 GSK923295 [34]. However, this difference could arise from the lack of filtering based on the number
98 of signaling chromosomes per cell.

99 Mad1 is recruited to metazoan kinetochores by Bub1 and the RZZ complex [35-37]. To quantify the
100 contribution of the RZZ complex, we depleted *ZW10* using RNA interference (RNAi) and then
101 quantified SAC protein recruitment as before. *ZW10* siRNA treatment lowered Bub1 and BubR1
102 recruitment by ~ 25%, as noted by others [38]. As expected, Mad1 recruitment was significantly
103 lower in both GSK923295 and nocodazole-treated cells (Figure S1). The number of Mad1
104 molecules recruited per Bub1 molecule was ~ 50% lower revealing the contribution of the RZZ
105 under these conditions. Although the number of Bub1 and BubR1 molecules per kinetochore was
106 also reduced, the two proteins were recruited in approximately equal amounts.

107 To test whether the inverse correlation is specific to HeLa cells, we examined Bub1 and BubR1
108 recruitment per kinetochore in hTERT-RPE1 cells. We released RPE-1 cells synchronized in G1/S
109 into media containing either nocodazole or GSK923295, and measured the total amounts of Bub1,
110 BubR1 recruited per kinetochore by immunofluorescence (Figure 1E). These measurements
111 show that the Bub1 amount per kinetochore in GSK923295-treated RPE-1 cells as ~1.6-fold
112 higher the Bub1 amount in nocodazole-treated cells; BubR1 amount was ~2.5-fold higher (Figure
113 1F). We did not quantify the amounts of Mad1 per kinetochore because a ring-like pool of Mad1
114 proximal to the spindle poles, especially in GSK923295-treated cells (see inset in Figure 1E),
115 prevented accurate quantification. These data demonstrate that the inverse correlation between
116 the amount of Bub1 and BubR1 per kinetochore and the number of signaling kinetochores is not
117 specific to HeLa or budding yeast cells. In fact, Bub1 and BubR1 show a similar degree of
118 enrichment at RPE-1 and HeLa kinetochores in GSK923295-treated cells.

119

120 **Mps1-mediated phosphorylation within signaling kinetochores is the same in nocodazole-**
121 **and GSK923295-treated cells**

122 Changes in the Mps1-mediated phosphoregulation of the kinetochore in GSK923295- and
123 nocodazole-treated cells may change SAC protein recruitment. Indeed, a prior study found that
124 the net Mps1-mediated phosphorylation decreased rather than increasing in GSK923295-treated
125 cells when compared to nocodazole-treated cells suggesting that SAC protein recruitment should
126 decrease in GSK923295-treated cells [34]. Therefore, we quantified the net Mps1 kinase activity
127 within the kinetochore using a recently developed FRET-based sensor (MPS1sen-KT) [34,39]. We
128 modified this sensor to use mNeonGreen/mScarlet-I as the acceptor/donor combination (Figure

129 S2A). Since the acceptor and the donor has a fixed 1:1 stoichiometry in the sensor, we used the
130 ratio between the green channel readout and the FRET channel readout (without correcting for
131 the cross-excitation of the acceptor fluorescence and the bleed-through of donor fluorescence)
132 as the normalized measurement of the FRET efficiency, which is positively correlated with the net
133 phosphorylation (Figure S2B-D).

134 We confirmed that MPS1sen-KT recruited to unaligned kinetochores in both nocodazole- and
135 GSK923295- treated cells had lower FRET efficiencies (higher activities of Mps1) compared to
136 kinetochores aligned at metaphase plates in GSK923295-treated cells (Figure S2D). Importantly,
137 we did not detect any difference in the net Mps1-mediated phosphorylation within unaligned
138 kinetochores in nocodazole- and GSK923295-treated cells irrespective of the drug concentration
139 used (Figure S2D). This divergence which may arise from different properties of the two cell lines
140 as was found in a panel of colorectal cancer cell lines [34]. In either case, the increased kinetochore
141 recruitment of SAC proteins in GSK929395-treated cells does not stem from increased Mps1-
142 mediated phosphorylation within the kinetochore.

143

144 **The number of MELT motifs per Knl1 controls Bub1, BubR1, and Mad1 recruitment to**
145 **signaling kinetochores**

146 We next studied how the number of MELT motifs per Knl1 affects the SAC protein recruitment.
147 We knocked down endogenous Knl1 using RNAi and replaced it with Knl1$^{\Delta}$-M3 or Knl1$^{\Delta}$-M3-M3,
148 which are mScarlet-I-tagged recombinant Knl1 versions containing three or six MELT motifs:
149 (Figure 2A) [5]. As before, we quantified Bub1, BubR1, and Mad1 signals at individual kinetochores
150 in cells treated with either GSK923295 or nocodazole (Figure 2B). For comparing the amounts of
151 proteins recruited under these conditions, we normalized all localized fluorescent intensities by
152 the average fluorescence signal per kinetochore of each protein in nocodazole-treated cells
153 expressing Knl1$^{\Delta}$-M3. As before, we used the labeled-to-unlabeled protein ratios to estimate the
154 total amount of protein per kinetochore (Figure 2C).

155 In the GSK923295-treted cells, Knl1$^{\Delta}$-M3 recruited ~ 1.4-times higher Bub1 per kinetochore
156 compared to nocodazole-treated cells. Knl1$^{\Delta}$-M3-M3 recruited more Bub1 than Knl1$^{\Delta}$-M3 under
157 both conditions. Importantly, Knl1$^{\Delta}$-M3-M3 recruited 2-fold higher Bub1 than Knl1$^{\Delta}$-M3 in
158 GSK923295-treated cells consistent with its 2-fold higher number of MELT motifs. These data
159 again highlight that the recruitment of SAC proteins per kinetochore is higher in cells containing
160 small numbers of signaling kinetochores. BubR1 and Mad1 recruitment showed similar trends.

161 Importantly, the total BubR1 recruitment per Knl1$^{\Delta}$-M3-M3 was 2-fold than Knl1$^{\Delta}$-M3 under both
162 conditions. BubR1 amount per Knl1$^{\Delta}$-M3 was 2-fold higher in GSK923295-treated cells compared
163 to nocodazole-treated cells, which is consistent with the increase in Bub1 recruitment by Knl1$^{\Delta}$-
164 M3 under the two conditions. Interestingly, total Mad1 recruitment by Knl1$^{\Delta}$-M3-M3 and Knl1$^{\Delta}$-M3
165 was similar in nocodazole-treated cells but increased by 5-fold in GSK923295-treated cells. The
166 kinetochore recruitment of the two recombinant Knl1's was very similar and cannot explain the
167 observed trends in SAC protein recruitment (Figure S3A).

168 As before, we combined these data with the immunoblotting quantitation to estimate the number
169 of molecules per Knl1 (Figure S3B). Knl1$^{\Delta}$-M3-M3 cells recruits ~ 5 ± 0.3 Bub1 molecules, but
170 only 3 ± 0.3 molecules in nocodazole-treated cells. These numbers are very similar to the
171 numbers of Bub1 molecules recruited by wild-type Knl1 under the two conditions (5 ± 0.9 and 3 ±
172 0.7 molecules respectively, see Figure S1), indicating that our estimates are internally consistent.
173 A prior study reported that HeLa kinetochores recruit 4-6 Bub1 molecules per kinetochore in
174 nocodazole-treated cells [5], whereas we find that there are 3 Bub1 molecules per Knl1 in
175 nocodazole-treated cells and 5 per kinetochore in GSK923295-treated cells. The reasons for this
176 discrepancy remain unclear.

177 These data provide several insights. First, they confirm that the number of MELT motifs per Knl1
178 strongly influences Bub1, BubR1, and Mad1 recruitment. Second, in the case of Bub1 and Mad1
179 this influence is detected only in GSK923295-treated cells containing small numbers of signaling
180 kinetochores. Third, Knl1$^{\Delta}$-M3-M3 recruits ~2-fold more BubR1 than Knl1$^{\Delta}$-M3 under both
181 conditions. Increased BubR1 recruitment to the kinetochore is likely to be functionally significant
182 because it promotes SAC signaling [14,23]. Mad1 recruitment is disproportionately high GSK923295-
183 treated cells, possibly because of changes in the contribution of the RZZ pathway to Mad1
184 recruitment [40]. Given the catalytic role of Mad1 in the rate-limiting step in the SAC signaling
185 cascade, the higher Mad1 recruitment may also increase the signaling activity of these
186 kinetochores. Therefore, we next tested whether the higher SAC protein recruitment by Knl1$^{\Delta}$-
187 M3-M3 translates into a stronger SAC and longer mitotic arrest durations.

188

189 **The number of MELT motifs per Knl1 affects the SAC signaling strength**

190 Previous studies concluded that the number of MELT motifs per Knl1 does not significantly
191 influence the duration of the SAC-mediated mitotic arrest unless the MELT motifs are weak in
192 their activity [5,13]. However, these studies characterized SAC signaling only in cells treated with

193 high doses of nocodazole. Our quantification shows that in the nocodazole-treated cells,
194 kinetochores containing Knl1$^{\Delta}$-M3-M3 recruit only modestly larger amounts of Bub1 and Mad1
195 compared to kinetochores containing Knl1$^{\Delta}$-M3. Therefore, the SAC signaling activity of both
196 types of kinetochores may have been similar in nocodazole-treated cells. A further complicating
197 factor is that one of the studies partially inhibited Mps1 during the experiment, which may have
198 masked differences in SAC signaling due to the two Knl1 versions [5].

199 Because of these considerations, we re-evaluated the strength of SAC signaling mediated by
200 Knl1$^{\Delta}$-M3 and Knl1$^{\Delta}$-M3-M3 specifically in GSK923295-treated cells. We used time-lapse imaging
201 to monitor mitotic progression in cells treated with different concentrations of GSK923295 to
202 achieve different degrees of CENP-E inhibition resulting in different durations of mitotic arrests.
203 In all cases, cells expressing Knl1$^{\Delta}$-M3-M3 arrested for significantly longer durations compared
204 to cells expressing Knl1$^{\Delta}$-M3 (Figure 2D-E). The same trend was observed when these cells were
205 treated with Taxol (Figure 2F). Thus, the number of MELT motifs in Knl1 can determine the
206 duration of checkpoint-induced mitotic delays in cells wherein a few signaling kinetochores sustain
207 the SAC. When combined with the results described in the previous section, this finding implies
208 that the higher recruitment of Bub1, BubR1, and Mad1 per kinetochore is correlated with a higher
209 SAC activity, and this correlation is readily detected only in when the mitotic cells contain small
210 numbers of signaling kinetochores [7].

211

212 **Bub1 over-expression increases recruitment of SAC proteins to the kinetochore**

213 A key question then what limits SAC protein recruitment to the kinetochore especially in
214 nocodazole-treated cells. Changes in phosphoregulation cannot explain the differences in SAC
215 protein recruitment under the two conditions studied here. One responsible factor may be the low
216 abundance of SAC proteins, especially Bub1, which is responsible for recruiting BubR1 and
217 Mad1. Bub1 overexpression results in higher Bub1 and Mad1 recruitment to the budding yeast
218 kinetochore [10]. Mad1 recruitment may also be limited by its own low abundance compared to
219 Bub1 and BubR1 [23]. Therefore, to assess SAC protein abundance, we used Fluorescence
220 Correlation Spectroscopy (FCS). We performed FCS measurements on mitotically cells arrested
221 either using MG132 or nocodazole. These measurements identified Mad1 is the protein with the
222 lowest abundance amongst the three SAC proteins. They also suggest that cytosolic
223 concentration of Bub1 is modestly lower in nocodazole-treated compared to MG132-treated cells
224 (Figure S3C).

225 To test whether higher Bub1 expression can lead to higher kinetochore recruitment of SAC
226 proteins, we exogenously expressed mNG-Bub1 in HeLa cells using a doxycycline-inducible
227 promoter (Figure S4A) and quantified Bub1, BubR1, and Mad1 recruitment per kinetochore in
228 cells treated with GSK923295 using immunofluorescence. As expected, mNG-Bub1 localization
229 at signaling kinetochores was detected only after doxycycline treatment (Figure 3A). To measure
230 the total amount of Bub1 per kinetochore, we fixed and stained these cells with anti-Bub1
231 antibodies. Fluorescence quantification confirmed that signaling kinetochores in the doxycycline-
232 treated cells recruited ~35% more Bub1 than signaling kinetochores in untreated cells (Figure 3A,
233 plot on the left). The kinetochores in the doxycycline-treated cells also recruited 26% more BubR1
234 (Figure 3A, middle plot), however, Mad1 amount per kinetochore did not change (Figure 3A, right
235 plot). Thus, signaling kinetochores in HeLa cells can recruit more Bub1 and BubR1 if more Bub1
236 is made available. However, Mad1 recruitment does not increase likely because of the low Mad1
237 abundance, although behavior of the RZZ pathway will also strongly influence Mad1 recruitment.

238

239 **Bub1 overexpression strengthens the SAC in the presence of a small numbers of signaling**
240 **kinetochores**

241 To test whether Bub1 overexpression results in longer delays in anaphase onset, we released
242 either untreated or doxycycline treated, G1/S synchronized cells into media containing 18-35 nM
243 GSK923295 and observed their mitotic progression (Figure 3B). We found that the doxycycline-
244 treated cells arrested for ~ 145 min on average, whereas the untreated cells arrested for ~ 94 min
245 under the same condition (Figure 3B, left, also see Supplementary Videos S1 and S2). To
246 understand the correlation between the expression level of exogenous Bub1 and the mitotic
247 duration, we plotted the mitotic duration against the cellular mNG signal in both cases (the
248 fluorescence values were normalized to the average mNG fluorescence per cell from samples not
249 treated with doxycycline, 3B right). As expected, there was no correlation between the cellular
250 mNG signal and mitotic duration in untreated cells (gray circles, Pearson's correlation coefficient
251 displayed at the top right of the figure). The mitotic duration of doxycycline-treated cells was
252 positively correlated with the mNG-Bub1 signal (orange circles in Figure 5B). It should be noted
253 that the mNG-Bub1 over-expression did not affect the mitotic progression of normally dividing
254 cells, and the degree of overexpression was also uncorrelated with the duration of mitosis (Figure
255 S4B-C). Thus, the longer mitotic duration seen in GSK923295-treated cells arises from higher
256 SAC signaling activity of the unaligned kinetochores.

257 We also examined whether Bub1 overexpression produces longer delays in anaphase onset in
258 nocodazole-treated cells (Figure 3C, also see Supplementary Videos S3 and S4). Interestingly,
259 the cellular mNG signal and the duration of mitosis did not statistically significant correlation in
260 this case (Figure 3C). The likely explanation for this observation is that even with increased Bub1
261 recruitment, the large number of signaling kinetochores cannot recruit higher amounts of
262 BubR1/MAD1 because of their depletion (implied by the reduced BubR1/MAD1 recruitment in the
263 nocodazole-treated cells, Figure 1). Therefore, the Bub1 overexpression does not translate into
264 more SAC signaling activity. In conclusion, increased Bub1 levels in HeLa cells increases Bub1
265 and BubR1 recruitment to the kinetochore and strengthens the SAC. Importantly, the effect on
266 SAC strength is detected only in GSK923295-treated cells, which contain small numbers of
267 signaling kinetochores.

268

269 **Partial depletion of Bub1 and BubR1 weakens the SAC in cells containing small numbers**
270 **of signaling kinetochores**

271 Mad1 abundance is lower than Bub1 abundance, which suggests that Mad1 availability should
272 also limit the signaling activity of individual kinetochores (Figure S3C). Because Mad1 over-
273 expression can weaken the SAC by depleting the Mad2 pool available for MCC formation, we
274 used a different approach [8,41-43]. Rather than over-expressing Mad1, we partially knocked down
275 Mad1-mNG using an siRNA against mNeonGreen in the genome-edited cell line heterozygous
276 for Mad1-mNG, and then quantified the duration of SAC-induced mitotic delays. We also lowered
277 mNG-Bub1 and mNG-BubR1 protein using the same strategy.

278 As expected, the mNG-tagged protein was significantly depleted by the mNeonGreen siRNA after
279 two days, whereas the unlabeled protein was unaffected (Figure 4A). To study the effect of a mild
280 depletion of an SAC protein on the signaling activity of the kinetochore, we treated the three cell
281 lines with mNG siRNA for one day and observed the effects of protein depletion on mitotic duration
282 in GSK923295- and nocodazole-treated cells. Quantification of mNG fluorescence signal from
283 mitotic cells revealed that the mNG RNAi reduce the level of the mNG-tagged protein by ~ 50%
284 (Figure 4B). In GSK923295-treated cells, it also significantly affected the mitotic progression
285 (Figure 4C, left). In the case of mNG-Bub1 and mNG-BubR1 depletion, the average duration of
286 mitosis decreased from ~ 1000 minutes to 300-500 minutes (Figure 4C). We also confirmed that
287 the partial depletion of BubR1 in GSK923295-treated cells resulted in chromosome
288 missegregation (Supplementary Videos S5 and S6). Mad1 depletion had a relatively minor effect
289 on mitotic duration: the average time in mitosis decreased from ~ 1000 minutes to 868 minutes

290 (Figure 4C). Interestingly, in nocodazole-treated cells, the partial depletion of all three proteins
291 did not significantly change the duration of mitosis (Figure 4C, right).

292 Many prior studies have shown that the depletion of Bub1 in HeLa cells has only a minor effect
293 on the duration of mitosis in nocodazole-treated cells [35,44-46]. Our results in nocodazole-treated
294 cells are consistent with these findings. Strikingly, we find that in GSK923295-treated cells even
295 a small (~ 20-40% on average) reduction in Bub1 or BubR1 level results in a significant decrease
296 in the duration of mitosis. This observation is consistent with our results involving Knl1$^{\Delta}$-M3 and
297 Knl1$^{\Delta}$-M3-M3 (Figure 2) and suggests that higher SAC protein recruitment to the kinetochore
298 results in higher SAC signaling activity. The likely reason why this is not seen in nocodazole-
299 treated cells is that the combined activity of a large number of signaling kinetochores masks
300 defects in the signaling activity of individual kinetochores [7].

301 In conclusion, HeLa and RPE-1 cells containing small numbers of signaling kinetochores recruit
302 significantly higher amounts of Bub1, BubR1, and Mad1 per signaling kinetochore compared to
303 cells containing many signaling kinetochores. The recruitment of all three proteins strongly
304 correlates with the number of MELT motifs in Knl1. This correlation is readily detected in cells
305 containing small numbers of signaling kinetochores; it cannot be detected in cells containing many
306 signaling kinetochores likely because of a shortage of unbound SAC proteins. Importantly, the
307 increased SAC protein recruitment per kinetochore, either due to the larger number of MELT
308 motifs or Bub1 over-expression, results in longer delays in anaphase onset. Conversely, partial
309 depletion of Bub1 and BubR1, but not Mad1, leads to shorter delays in anaphase onset in the
310 presence of a small number of signaling kinetochores.

311 The inverse correlation between the recruitment level of SAC proteins at a signaling kinetochore
312 and the total number of signaling kinetochores in a cell is likely to be biologically significant (Figure
313 4D). In human cells, the number of signaling kinetochores drops by almost two orders of
314 magnitude: from ~ 92 following nuclear envelop break-down to a few or just one in prometaphase.
315 If the amount of MCC in the cell scales linearly with the number of signaling kinetochores, the
316 nearly 100-fold drop in the number of kinetochores will result in a similar drop in the MCC creating
317 the possibility of a premature anaphase onset. Pre-mitotic MCC generation at the nuclear envelop
318 also buffers SAC signaling activity of the kinetochores [47]. However, the strong decrease in the
319 duration of mitotic arrest in cells expressing Knl1$^{\Delta}$-M3 or cells with partial Bub1 depletion suggests
320 that the buffering mechanism cannot compensate for lower signaling activity of kinetochores.
321 Instead, our data suggest that as the number of signaling kinetochores drops, the availability of
322 SAC signaling proteins, especially Bub1, increases, and enables the remaining signaling

323 kinetochores to recruit more SAC proteins. Consequently, the signaling strength of each
324 kinetochore will become inversely correlated to the number of signaling kinetochores in the cell.
325 Additionally, synergistic signaling by the Knl1 phosphodomain under this condition may further
326 strengthen the signaling activity of these remaining kinetochores [48].

327 Our results also raise additional questions requiring further investigation. First, it remains unclear
328 why kinetochores in HeLa cells and other eukaryotes use only a small fraction of their signaling
329 strength. One possibility is that this modulation of the signaling strength of the kinetochore
330 represents a compromise for balancing SAC signaling strength with its responsiveness to
331 silencing mechanisms [7]. Higher Bub1 expression may also have drawbacks in other aspects of
332 mitosis and cell biology [49]. Finally, these results bring into focus the contribution of perturbations
333 or imbalance in the expression levels of SAC proteins on chromosome missegregation commonly
334 seen in cancer cells [50].

335

336

337 **Acknowledgements**

338 This work was supported by R35-GM126983 from the National Institute of General Medical
339 Sciences to APJ. We thank Dr. Makayev for sharing the HeLa A-12 parental cell line, Dr. Geert
340 Kops for kindly sharing the design details for the MPS1sen-KT construct, and Dr. Taylor for
341 sharing anti-Bub1 antibodies. We also thank Dr. Iain Cheeseman and Dr. Mara Duncan for
342 feedback on the manuscript and useful discussion.

343 **Materials and Methods**
344
345 **Cell culture**
346 HeLa A12 cells (a kind gift from the Makeyev lab) were grown in DMEM media supplemented with
347 10% fetal bovine serum (FBS), Pen-Strep, 25 mM HEPES, and 1x GlutaMAX at 37 °C and 5%
348 CO_2. 0.5-2 µg/ml Puromycin or 10 µg/ml Blasticidin was used as needed. To express recombinant
349 proteins, we modified a bicistronic vector designed by the Makeyev lab as necessary [51]. The
350 modified vectors were transfected into HeLa A12 cells that have the *LoxP*-Blasticidin-*Lox2272*
351 cassette engineered into their genome. Transformed cells were pooled and used for further
352 experimentation. The methodology used to construct the genome-edited HeLa A12 cell lines has
353 been described in detail in [52].
354 Imaging experiments were performed in Fluorobrite media supplemented with FBS, Pen-Strep,
355 HEPES as noted above. G1/S synchronization was achieved using a double thymidine block
356 procedure (2.5 mM thymidine). On the day of imaging, cells were released from the second block
357 and treated with either nocodazole or GSK923295 ~ 1.5 hours prior to imaging.
358
359 **Immunoblotting**

360 For the quantitative immunoblot analysis shown in Figure S1, cells were synchronized using a
361 single thymidine block (2.5 mM thymidine) for 24 hours. The cells were released into media
362 containing 660 nM Nocodazole and harvested 15 hours post release. Anti-Bub1 (A300-373A,
363 Bethyl Laboratories), anti-BubR1 (A300-386A, Bethyl Laboratories), and anti-Mad1 (ab184560,
364 Abcam) primary antibodies were used to probe membranes at a dilution of 1:1000. Alexa Fluor
365 633-conjugated secondary antibodies (Goat anti-Mouse, Invitrogen A21052 or Goat anti-Rabbit,
366 Invitrogen A21071 as appropriate) were used at a 1:15000 dilution.

367 For immunoblots in Figures 4A, S2A, and S4A: To acquire unsynchronized HeLa-A12 cells
368 lysates, cells were either scraped off the dish surface or trypsinized. To acquired mitotic HeLa-
369 A12 cells, cells were first synchronized in G1/S with 2.5 mM thymidine and then arrested in mitosis
370 with 330 nM of nocodazole for 16 h before mitotic shake-off. Mitotic cells were then washed once
371 by phosphate-buffered saline (Gibco), pelleted down, and chilled on ice. Lysis was performed by
372 directly adding 2x Laemmli sample buffer (supplemented by 2-mercaptoethanol, Bio-Rad
373 Laboratories) at a ratio of 1 µL per 0.1 mg of cell pellets and pipetting up and down. Lysates were
374 boiled immediately afterward for 10 min and then chilled on ice. 8 µL of supernatant was loaded
375 onto each lane of a 15-well, 0.75-mm SDS-PAGE mini gel.

376 Primary antibodies used included anti-BUBR1 (Bethyl Laboratories A300-995A, 1 : 1000), anti-
377 MAD1 (GeneTex GTX109519, 1 : 2000), anti-CDC20 (Santa Cruz Biotechnology sc-13162, 1 :
378 200), anti-BUB3 (Sigma-Aldrich B7811, 1 : 500), anti-GAPDH (Proteintech 60004-1-Ig, 1 : 5000).

379

380 **RNA interference**

381 Cells were transfected with siRNA in the morning. 2.5 mM of thymidine was added 8 h later and
382 cells were incubated overnight. The next morning, cells were released from the thymidine block
383 into fresh media. This sequence was then repeated once and cells were released into
384 FluoroBrite™ DMEM (Gibco) supplemented with 9% (by volume) of FBS and 1× GlutaMAX and
385 incubated for 6 h before the addition of mitotic drugs. Drugs were left to take effect for 1 h before
386 imaging.

387 Sense-strand sequences and working concentrations of small interfering RNA duplexes (siRNAs)
388 used in this study include the *SPC25* siRNA (5'- GCCUGCGAAGCAUUGUCCUACAUAA-3', 40
389 nM [53]), *BUBR1* siRNA (5'-GAUGGUGAAUUGUGGAAUA-3', 40 nM [54]), *BUB1* siRNA (5'-
390 CGAAGAGUGAUCACGAUUU-3', 40 nM [55]), mNeonGreen siRNA (5'-
391 GAGCUGAAGCACUCCAAGACA-3', 40 nM) and the *ZW10* siRNA (5'-
392 UGAUCAAUGUGCUGUUCAA-3', 100 nM [38]). The siRNAs against all five B56 isoforms were
393 taken from the second pool in [56]. Desalted siRNA duplexes modified by double-deoxythymidine
394 overhangs at 3'-ends of both strands were synthesized by Sigma. The AllStar siRNA (QIAGEN)
395 was used for the negative control. All siRNAs were transfected into the cells via Lipofectamine
396 RNAiMAX (Invitrogen).

397

398 **Live-cell imaging**

399 Cells were plated in a Nunc Lab-Tek II chambered cover glass (Thermo Scientific) or a 35-mm
400 cover glass-bottomed dish (MatTek) and treated with drugs and/or siRNAs as described above.
401 For imaging, the chambered cover glass or the cover glass-bottomed dish was loaded into a CU-
402 501 temperature and gas control system (Live Cell Instrument). The sample holder was
403 maintained at 37°C and ventilated by humidified 5% of CO_2 and the objective was maintained at
404 37°C by a heating band.

405 MPS1sen-KT FRET and immunofluorescence experiments were performed on a Nikon Eclipse
406 Ti-E/B inverted microscope, with a CFI Plan Apochromat Lambda 100×, 1.45 NA oil objective
407 (Nikon). The microscope was equipped with an H117E1 motorized stage (Prior Scientific) and a

408 NanoScanZ 100 piezo stage (Prior Scientific). A SPECTRA 5-LCR-XA Light Engine (Lumencor)
409 served as the excitation light source. The 475 nm-centered band of excitation light was used for
410 the green channel and the 575/30nm-filtered band of excitation light was used for the red channel.
411 An ET-EGFP/mCherry filter cube (Chroma Technology) was used as the dichroic mirror, where
412 the built-in emission filter on the cube has been removed. Emission light in the red channel was
413 filtered by an ET632/60m (Chroma Technology). Emission light in the green channel was filtered
414 by an ET525/50m (Chroma Technology). Emission filters were mounted on a high-speed filter
415 wheel (Prior Scientific) positioned in the light path. Images were acquired with an iXon3 EMCCD
416 camera (Andor Technology) operating in the conventional CCD mode. Signaling kinetochores in
417 GSK923295-treated cells were identified by their polar positioning and the enrichment of localized
418 SAC proteins on them.

419 The FRET measurement with MPS1sen-KT was performed on a Nikon Eclipse TiE/B inverted
420 microscope, with a CFI Plan Apochromat VC 100×, 1.40 NA oil objective (Nikon). The microscope
421 was equipped with an H117E1 motorized stage (Prior Scientific), a NanoScanZ 100 piezo stage
422 (Prior Scientific), and an X-Light V2 L-FOV confocal unit with 60-μm pinholes (CrestOptics). A
423 CELESTA Light Engine (Lumencor) served as the excitation laser source. The 477-nm line (at
424 25% power with an exposure time of 400ms for each frame) was used for both the green and the
425 FRET channels and the 546-nm line (at 50% power with an exposure time of 400ms for each
426 frame) was used for the red channel. A ZT488/543rpc (Chroma Technology) was used as the
427 dichroic mirror. Emission through both the red and the FRET channels was filtered by an
428 ET605/52m (Chroma Technology) while emission through the green channel was filtered by an
429 ET525/36m (Chroma Technology). Images were acquired by a Prime 95B 25mm sCMOS camera
430 (Teledyne Photometrics).

431 Time-lapse live-cell imaging related to the knockdown-rescue experiments was performed on an
432 ImageXpress Nano Automated Imaging System (Molecular Devices). A SOLA Light Engine
433 (Lumencor) served as the excitation light source. Cells were plated on 24-well cell imaging plates
434 (black plate with treated glass bottom, Eppendorf) and treated with drugs and/or siRNAs
435 accordingly. Input humidified 5% CO_2 flow was maintained at around 19 psi and the environment
436 chamber was maintained at 37°C. All SAC proteins tagged by mNeonGreen (BUBR1, BUB1, and
437 MAD1) feature inhomogeneous distributions between the cytosol and the nucleus/nuclear
438 envelope in the prophase (data not shown). In principle, they can indicate the accurate timing of
439 the nuclear envelope breakdown (NEBD) in each cell during the time-lapse imaging. However,
440 due to the resolution limit and for consistency, we determined mitotic duration mainly based on

441 cell morphology (from rounding-up at the NEBD to elongation at the anaphase onset) from
442 transmitted-light images. This was facilitated by the semi-automatic image analysis pipeline
443 available at https://github.com/CreLox/IXNAnalysis [48].

444

445 **Immunofluorescence**

446 Hela cells that exogenously expressing mNG-Bub1 were plated on a 12-mm coverslip and
447 synchronized by thymidine (2.5 mM for 8 hours) followed by RO3306 treatment (15 nM for 20
448 hours). G2/M arrested cells were washed three times with PBS and released into media
449 containing GSK923295 (236 nM) for 4 hours) to get arrested in Mitosis. For immunolabeling, the
450 cells were pre-extracted with 0.5% Triton X-100 in PHEM (240 mM Pipes, 100 mM HEPES, 8 mM
451 $MgCl_2$ and 40 mM EGTA) and then fixed with 4% PFA for 10 min. The coverslips were washed
452 three times with PHEM buffer and blocked for 30 min at room-temperature with 5% Donkey serum.
453 Next, the coverslips were incubated in anti-Mad1 (1:1000, Sigma M80691), anti-Bub1 (1:500,
454 Thermo A300-373A), or anti-BubR1 (1:1000, Thermo Scientific A300-373A) over night at 4°C.
455 The next day, the coverslips were washed 4 times with PHEM containing 0.05% Tween-20 and
456 incubated with appropriate Alexa Fluor 633-conjugated secondary antibodies (Goat anti-Mouse,
457 Invitrogen A21052 or Goat anti-Rabbit, Invitrogen A21071) at a 1:10000 dilution for 45 min at
458 room temperature in the dark. Following secondary antibody labeling, the coverslips were washed
459 four times and mounted in an antifade solution (ProLong; Molecular Probes).

460 Immunofluorescence images were acquired on the spinning disk confocal microscope described
461 above. For each field of view, 31 *z*-sections were acquired at 0.2-μm steps.

462

463 **Quantification of kinetochore-localized fluorescence signal**

464 Quantification of the kinetochore-localized fluorescence signal was performed using a custom
465 graphical user interface written in MATLAB. The methodology has been described previously [11,53].
466 Briefly, individual kinetochores were identified in the mCherry channel based on the Spc25-
467 mCherry fluorescence. A 6×6-pixel box was drawn centered on the maximum intensity pixel in
468 the in-focus mCherry plane, and the mNG intensity of all the pixels within this box was summed
469 to obtain the mNG fluorescence signal for that kinetochore. The local background was defined as
470 the median intensity value of the perimeter pixel intensities in a 10×10 pixel box concentric with
471 the 6×6 pixel kinetochore box.

472 For immunofluorescence quantification involving both RPE-1 and HeLa cells, anti-ACA antibodies
473 probed with Alexa Fluor 488-conjugated secondary antibodies were used to identify the
474 centromeres. Alexa Fluor 633-conjugated secondary antibodies were used to visualize primary
475 antibodies against the respective SAC proteins.
476
477 **Fluorescence correlation spectroscopy (FCS)**

478 The total number of fluorophores in a homogeneous solution is $N_{total} := N_A c V_{total}$, where N_A is the
479 Avogadro constant, c is the molar concentration of the fluorophore, and V_{total} is the total volume
480 of the solution. The probability that a specific fluorophore molecule is within the excitation volume
481 $V_0 (\ll V_{total})$ at any given time is $p_0 := V_0/V_{total} \ll 1$. For freely diffusive fluorophores in a diluted
482 solution, whether or not a specific fluorophore is within the excitation volume is independent of
483 each other. Thus, the number of fluorophores inside the excitation volume at any given time N_0
484 has a binomial distribution $B(N_{total}, p_0)$. Therefore,

485
$$G_0 := \frac{\sigma_{N_0}^2}{\langle N_0 \rangle^2} = \frac{1 - p_0}{N_{\text{total}} p_0} \approx \frac{1}{N_{\text{A}} c V_0}.$$

486 Under a fixed live-cell imaging setup [which includes the microscope (its alignment and the
487 objective), the wavelength of the excitation light, the thickness of the coverslip (affecting the actual
488 working distance), and the refractive index of the cytosol], V_0 is fixed. Therefore, G_0 is inversely
489 proportional to the molar concentration of the fluorophore. The average number (or the variance
490 of the number) of fluorophores inside the excitation volume observed over a long period should
491 be close to the theoretical mean $\langle N_0 \rangle$ (or the theoretical variance σ^2_{N0}).

492 All FCS data were collected on an Alba v5 Laser Scanning Microscope (ISS), connected to an
493 Olympus IX81 inverted microscope main body [equipped with a UPLSAPO60XW objective (1.2
494 NA, Olympus)]. A Fianium WL-SC-400-8 laser (NKT Photonics) with an acoustooptic tunable filter
495 was used to generate excitation pulses at a wavelength of 488 nm and a frequency of around 20
496 MHz. Excitation light was further filtered by a Z405/488/561/635rpc quadband dichroic mirror
497 (Chroma). Emission went through a 655DCSPXR short-pass dichroic mirror (Chroma) and an
498 FF01-531/40-25 filter (Semrock) and was finally detected by an SPCM-AQRH-15 avalanche
499 photodiode (Perkin Elmer). The time-correlated single photon counting module to register
500 detected photon events to excitation pulses was SPC830 (Becker & Hickl). Data acquisition was
501 facilitated by VistaVision (ISS). The excitation volume (V_0) was calibrated by taking FCS data from
502 TetraSpeck™ microspheres (0.1 μm, Invitrogen) of known concentrations.

503 **Statistical analysis**

504 Statistical analysis was conducted using GraphPad Prism version 9.

505

506

507 **References**

508 1. Musacchio, A. (2015). The Molecular Biology of Spindle Assembly Checkpoint Signaling
509 Dynamics. Curr Biol *25*, R1002-1018. 10.1016/j.cub.2015.08.051.
510 2. Lara-Gonzalez, P., Pines, J., and Desai, A. (2021). Spindle assembly checkpoint activation
511 and silencing at kinetochores. Semin. Cell Dev. Biol. *117*, 86-98.
512 10.1016/j.semcdb.2021.06.009.
513 3. Izawa, D., and Pines, J. (2015). The mitotic checkpoint complex binds a second CDC20 to
514 inhibit active APC/C. Nature *517*, 631-634. 10.1038/nature13911.
515 4. Sudakin, V., Chan, G.K., and Yen, T.J. (2001). Checkpoint inhibition of the APC/C in HeLa
516 cells is mediated by a complex of BUBR1, BUB3, CDC20, and MAD2. J Cell Biol *154*, 925-
517 936. 10.1083/jcb.200102093.
518 5. Vleugel, M., Omerzu, M., Groenewold, V., Hadders, M.A., Lens, S.M., and Kops, G.J.
519 (2015). Sequential multisite phospho-regulation of KNL1-BUB3 interfaces at mitotic
520 kinetochores. Mol Cell *57*, 824-835. 10.1016/j.molcel.2014.12.036.
521 6. Collin, P., Nashchekina, O., Walker, R., and Pines, J. (2013). The spindle assembly
522 checkpoint works like a rheostat rather than a toggle switch. Nat Cell Biol *15*, 1378-1385.
523 10.1038/ncb2855.
524 7. Roy, B., Han, S.J.Y., Fontan, A.N., and Joglekar, A.P. (2020). The copy-number and varied
525 strength of MELT motifs in Spc105 balance the strength and responsiveness of the Spindle
526 Assembly Checkpoint. Elife *9*. 10.7554/eLife.55096.
527 8. Heinrich, S., Geissen, E.M., Kamenz, J., Trautmann, S., Widmer, C., Drewe, P., Knop, M.,
528 Radde, N., Hasenauer, J., and Hauf, S. (2013). Determinants of robustness in spindle
529 assembly checkpoint signalling. Nat Cell Biol *15*, 1328-1339. 10.1038/ncb2864.
530 9. Gelens, L., Qian, J., Bollen, M., and Saurin, A.T. (2018). The Importance of Kinase-
531 Phosphatase Integration: Lessons from Mitosis. Trends Cell Biol *28*, 6-21.
532 10.1016/j.tcb.2017.09.005.
533 10. Aravamudhan, P., Chen, R., Roy, B., Sim, J., and Joglekar, A.P. (2016). Dual mechanisms
534 regulate the recruitment of spindle assembly checkpoint proteins to the budding yeast
535 kinetochore. Mol Biol Cell *27*, 3405-3417. 10.1091/mbc.E16-01-0007.
536 11. Hoffman, D.B., Pearson, C.G., Yen, T.J., Howell, B.J., and Salmon, E.D. (2001). Microtubule-
537 dependent changes in assembly of microtubule motor proteins and mitotic spindle
538 checkpoint proteins at PtK1 kinetochores. Mol Biol Cell *12*, 1995-2009.
539 12. Vleugel, M., Tromer, E., Omerzu, M., Groenewold, V., Nijenhuis, W., Snel, B., and Kops,
540 G.J. (2013). Arrayed BUB recruitment modules in the kinetochore scaffold KNL1 promote
541 accurate chromosome segregation. J Cell Biol *203*, 943-955. 10.1083/jcb.201307016.
542 13. Zhang, G., Lischetti, T., and Nilsson, J. (2014). A minimal number of MELT repeats supports
543 all the functions of KNL1 in chromosome segregation. J Cell Sci *127*, 871-884.
544 10.1242/jcs.139725.
545 14. Piano, V., Alex, A., Stege, P., Maffini, S., Stoppiello, G.A., Huis In 't Veld, P.J., Vetter, I.R.,
546 and Musacchio, A. (2021). CDC20 assists its catalytic incorporation in the mitotic
547 checkpoint complex. Science *371*, 67-71. 10.1126/science.abc1152.

548 15. Primorac, I., Weir, J.R., Chiroli, E., Gross, F., Hoffmann, I., van Gerwen, S., Ciliberto, A., and
549 Musacchio, A. (2013). Bub3 reads phosphorylated MELT repeats to promote spindle
550 assembly checkpoint signaling. Elife *2*, e01030. 10.7554/eLife.01030.
551 16. London, N., and Biggins, S. (2014). Mad1 kinetochore recruitment by Mps1-mediated
552 phosphorylation of Bub1 signals the spindle checkpoint. Genes Dev *28*, 140-152.
553 10.1101/gad.233700.113.
554 17. London, N., Ceto, S., Ranish, J.A., and Biggins, S. (2012). Phosphoregulation of Spc105 by
555 Mps1 and PP1 regulates Bub1 localization to kinetochores. Curr Biol *22*, 900-906.
556 10.1016/j.cub.2012.03.052.
557 18. Shepperd, L.A., Meadows, J.C., Sochaj, A.M., Lancaster, T.C., Zou, J., Buttrick, G.J.,
558 Rappsilber, J., Hardwick, K.G., and Millar, J.B. (2012). Phosphodependent recruitment of
559 Bub1 and Bub3 to Spc7/KNL1 by Mph1 kinase maintains the spindle checkpoint. Curr Biol
560 *22*, 891-899. 10.1016/j.cub.2012.03.051.
561 19. Ji, Z., Gao, H., Jia, L., Li, B., and Yu, H. (2017). A sequential multi-target Mps1
562 phosphorylation cascade promotes spindle checkpoint signaling. Elife *6*.
563 10.7554/eLife.22513.
564 20. Faesen, A.C., Thanasoula, M., Maffini, S., Breit, C., Muller, F., van Gerwen, S., Bange, T.,
565 and Musacchio, A. (2017). Basis of catalytic assembly of the mitotic checkpoint complex.
566 Nature. 10.1038/nature21384.
567 21. Lara-Gonzalez, P., Kim, T., Oegema, K., Corbett, K., and Desai, A. (2021). A tripartite
568 mechanism catalyzes Mad2-Cdc20 assembly at unattached kinetochores. Science *371*, 64-
569 67. 10.1126/science.abc1424.
570 22. Shaner, N.C., Lambert, G.G., Chammas, A., Ni, Y., Cranfill, P.J., Baird, M.A., Sell, B.R., Allen,
571 J.R., Day, R.N., Israelsson, M., et al. (2013). A bright monomeric green fluorescent protein
572 derived from Branchiostoma lanceolatum. Nat Methods *10*, 407-409.
573 10.1038/nmeth.2413.
574 23. Banerjee, A., Chen, C., Humphrey, L., Tyson, J.J., and Joglekar, A.P. (2022). BubR1
575 recruitment to the kinetochore via Bub1 enhances spindle assembly checkpoint signaling.
576 Mol Biol Cell *33*, br16. 10.1091/mbc.E22-03-0085.
577 24. Qian, X., McDonald, A., Zhou, H.J., Adams, N.D., Parrish, C.A., Duffy, K.J., Fitch, D.M.,
578 Tedesco, R., Ashcraft, L.W., Yao, B., et al. (2010). Discovery of the First Potent and
579 Selective Inhibitor of Centromere-Associated Protein E: GSK923295. ACS Med Chem Lett
580 *1*, 30-34. 10.1021/ml900018m.
581 25. Kuhn, J., and Dumont, S. (2019). Mammalian kinetochores count attached microtubules
582 in a sensitive and switch-like manner. J Cell Biol *218*, 3583-3596. 10.1083/jcb.201902105.
583 26. Krefman, N.I., Drubin, D.G., and Barnes, G. (2015). Control of the spindle checkpoint by
584 lateral kinetochore attachment and limited Mad1 recruitment. Mol Biol Cell.
585 10.1091/mbc.E15-05-0276.
586 27. Fischer, E.S., Yu, C.W.H., Bellini, D., McLaughlin, S.H., Orr, C.M., Wagner, A., Freund,
587 S.M.V., and Barford, D. (2021). Molecular mechanism of Mad1 kinetochore targeting by
588 phosphorylated Bub1. EMBO Rep, e52242. 10.15252/embr.202052242.
589 28. Vleugel, M., Hoek, T.A., Tromer, E., Sliedrecht, T., Groenewold, V., Omerzu, M., and Kops,
590 G.J. (2015). Dissecting the roles of human BUB1 in the spindle assembly checkpoint. J Cell
591 Sci *128*, 2975-2982. 10.1242/jcs.169821.

592 29. Zhang, G., Lischetti, T., Hayward, D.G., and Nilsson, J. (2015). Distinct domains in Bub1
593 localize RZZ and BubR1 to kinetochores to regulate the checkpoint. Nat Commun *6*, 7162.
594 10.1038/ncomms8162.
595 30. Zhang, G., Kruse, T., Lopez-Mendez, B., Sylvestersen, K.B., Garvanska, D.H., Schopper, S.,
596 Nielsen, M.L., and Nilsson, J. (2017). Bub1 positions Mad1 close to KNL1 MELT repeats to
597 promote checkpoint signalling. Nat Commun *8*, 15822. 10.1038/ncomms15822.
598 31. Zhang, G., Mendez, B.L., Sedgwick, G.G., and Nilsson, J. (2016). Two functionally distinct
599 kinetochore pools of BubR1 ensure accurate chromosome segregation. Nat Commun *7*,
600 12256. 10.1038/ncomms12256.
601 32. Overlack, K., Primorac, I., Vleugel, M., Krenn, V., Maffini, S., Hoffmann, I., Kops, G.J., and
602 Musacchio, A. (2015). A molecular basis for the differential roles of Bub1 and BubR1 in
603 the spindle assembly checkpoint. Elife *4*, e05269. 10.7554/eLife.05269.
604 33. Suzuki, A., Badger, B.L., and Salmon, E.D. (2015). A quantitative description of Ndc80
605 complex linkage to human kinetochores. Nat Commun *6*, 8161. 10.1038/ncomms9161.
606 34. Kuijt, T.E.F., Lambers, M.L.A., Weterings, S., Ponsioen, B., Bolhaqueiro, A.C.F., Staijen,
607 D.H.M., and Kops, G. (2020). A Biosensor for the Mitotic Kinase MPS1 Reveals
608 Spatiotemporal Activity Dynamics and Regulation. Curr Biol *30*, 3862-3870 e3866.
609 10.1016/j.cub.2020.07.062.
610 35. Rodriguez-Rodriguez, J.A., Lewis, C., McKinley, K.L., Sikirzhytski, V., Corona, J.,
611 Maciejowski, J., Khodjakov, A., Cheeseman, I.M., and Jallepalli, P.V. (2018). Distinct Roles
612 of RZZ and Bub1-KNL1 in Mitotic Checkpoint Signaling and Kinetochore Expansion. Curr
613 Biol *28*, 3422-3429 e3425. 10.1016/j.cub.2018.10.006.
614 36. Pereira, C., Reis, R.M., Gama, J.B., Celestino, R., Cheerambathur, D.K., Carvalho, A.X., and
615 Gassmann, R. (2018). Self-Assembly of the RZZ Complex into Filaments Drives Kinetochore
616 Expansion in the Absence of Microtubule Attachment. Curr Biol *28*, 3408-3421 e3408.
617 10.1016/j.cub.2018.08.056.
618 37. Silio, V., McAinsh, A.D., and Millar, J.B. (2015). KNL1-Bubs and RZZ Provide Two Separable
619 Pathways for Checkpoint Activation at Human Kinetochores. Dev Cell *35*, 600-613.
620 10.1016/j.devcel.2015.11.012.
621 38. Kops, G.J., Kim, Y., Weaver, B.A., Mao, Y., McLeod, I., Yates, J.R., 3rd, Tagaya, M., and
622 Cleveland, D.W. (2005). ZW10 links mitotic checkpoint signaling to the structural
623 kinetochore. J Cell Biol *169*, 49-60. 10.1083/jcb.200411118.
624 39. Violin, J.D., Zhang, J., Tsien, R.Y., and Newton, A.C. (2003). A genetically encoded
625 fluorescent reporter reveals oscillatory phosphorylation by protein kinase C. J Cell Biol
626 *161*, 899-909. 10.1083/jcb.200302125.
627 40. Sacristan, C., Ahmad, M.U.D., Keller, J., Fermie, J., Groenewold, V., Tromer, E., Fish, A.,
628 Melero, R., Carazo, J.M., Klumperman, J., et al. (2018). Dynamic kinetochore size
629 regulation promotes microtubule capture and chromosome biorientation in mitosis. Nat
630 Cell Biol *20*, 800-810. 10.1038/s41556-018-0130-3.
631 41. Chen, R.-H., Brady, D.M., Smith, D., Murray, A.W., and Hardwick, K.G. (1999). The Spindle
632 Checkpoint of Budding Yeast Depends on a Tight Complex between the Mad1 and Mad2
633 Proteins. Molecular Biology of the Cell *10*, 2607-2618.
634 42. Ryan, S.D., Britigan, E.M., Zasadil, L.M., Witte, K., Audhya, A., Roopra, A., and Weaver,
635 B.A. (2012). Up-regulation of the mitotic checkpoint component Mad1 causes

636 chromosomal instability and resistance to microtubule poisons. Proc Natl Acad Sci USA
637 *109*, E2205-2214. 10.1073/pnas.1201911109.
638 43. Barnhart, E.L., Dorer, R.K., Murray, A.W., and Schuyler, S.C. (2011). Reduced Mad2
639 expression keeps relaxed kinetochores from arresting budding yeast in mitosis. Mol Biol
640 Cell *22*, 2448-2457. 10.1091/mbc.E09-01-0029.
641 44. Morrow, C.J., Tighe, A., Johnson, V.L., Scott, M.I., Ditchfield, C., and Taylor, S.S. (2005).
642 Bub1 and aurora B cooperate to maintain BubR1-mediated inhibition of APC/CCdc20. J
643 Cell Sci *118*, 3639-3652.
644 45. Raaijmakers, J.A., van Heesbeen, R., Blomen, V.A., Janssen, L.M.E., van Diemen, F.,
645 Brummelkamp, T.R., and Medema, R.H. (2018). BUB1 Is Essential for the Viability of
646 Human Cells in which the Spindle Assembly Checkpoint Is Compromised. Cell Rep *22*,
647 1424-1438. 10.1016/j.celrep.2018.01.034.
648 46. Zhang, G., Kruse, T., Guasch Boldu, C., Garvanska, D.H., Coscia, F., Mann, M., Barisic, M.,
649 and Nilsson, J. (2019). Efficient mitotic checkpoint signaling depends on integrated
650 activities of Bub1 and the RZZ complex. EMBO J *38*. 10.15252/embj.2018100977.
651 47. Rodriguez-Bravo, V., Maciejowski, J., Corona, J., Buch, H.K., Collin, P., Kanemaki, M.T.,
652 Shah, J.V., and Jallepalli, P.V. (2014). Nuclear pores protect genome integrity by
653 assembling a premitotic and Mad1-dependent anaphase inhibitor. Cell *156*, 1017-1031.
654 10.1016/j.cell.2014.01.010.
655 48. Chen, C., Whitney, I.P., Banerjee, A., Sacristan, C., Sekhri, P., Kern, D.M., Fontan, A., Kops,
656 G., Tyson, J.J., Cheeseman, I.M., and Joglekar, A.P. (2019). Ectopic Activation of the
657 Spindle Assembly Checkpoint Signaling Cascade Reveals Its Biochemical Design. Curr Biol
658 *29*, 104-119 e110. 10.1016/j.cub.2018.11.054.
659 49. Li, F., Kim, H., Ji, Z., Zhang, T., Chen, B., Ge, Y., Hu, Y., Feng, X., Han, X., Xu, H., et al. (2018).
660 The BUB3-BUB1 Complex Promotes Telomere DNA Replication. Mol Cell *70*, 395-407
661 e394. 10.1016/j.molcel.2018.03.032.
662 50. Cohen-Sharir, Y., McFarland, J.M., Abdusamad, M., Marquis, C., Bernhard, S.V.,
663 Kazachkova, M., Tang, H., Ippolito, M.R., Laue, K., Zerbib, J., et al. (2021). Aneuploidy
664 renders cancer cells vulnerable to mitotic checkpoint inhibition. Nature *590*, 486-491.
665 10.1038/s41586-020-03114-6.
666 51. Khandelia, P., Yap, K., and Makeyev, E.V. (2011). Streamlined platform for short hairpin
667 RNA interference and transgenesis in cultured mammalian cells. Proc Natl Acad Sci USA
668 *108*, 12799-12804. 10.1073/pnas.1103532108.
669 52. Banerjee, A., Chen, C., Humphrey, L., Tyson, J.J., and Joglekar, A.P. (2021). BubR1
670 recruitment to the kinetochore via Bub1 enhances Spindle Assembly Checkpoint
671 signaling. bioRxiv, 2021.2008.2012.456107. 10.1101/2021.08.12.456107.
672 53. Kukreja, A.A., Kavuri, S., and Joglekar, A.P. (2020). Microtubule Attachment and
673 Centromeric Tension Shape the Protein Architecture of the Human Kinetochore. Curr Biol
674 *30*, 4869-4881 e4865. 10.1016/j.cub.2020.09.038.
675 54. Nilsson, J., Yekezare, M., Minshull, J., and Pines, J. (2008). The APC/C maintains the spindle
676 assembly checkpoint by targeting Cdc20 for destruction. Nat Cell Biol *10*, 1411-1420.
677 10.1038/ncb1799.

678 55. Yang, C., Wang, H., Xu, Y., Brinkman, K.L., Ishiyama, H., Wong, S.T., and Xu, B. (2012). The
679 kinetochore protein Bub1 participates in the DNA damage response. DNA repair *11*, 185-
680 191. 10.1016/j.dnarep.2011.10.018.
681 56. Foley, E.A., Maldonado, M., and Kapoor, T.M. (2011). Formation of stable attachments
682 between kinetochores and microtubules depends on the B56-PP2A phosphatase. Nat Cell
683 Biol *13*, 1265-1271. 10.1038/ncb2327.
684 57. Ries, J., and Schwille, P. (2012). Fluorescence correlation spectroscopy. Bioessays *34*, 361-
685 368. https://doi.org/10.1002/bies.201100111.

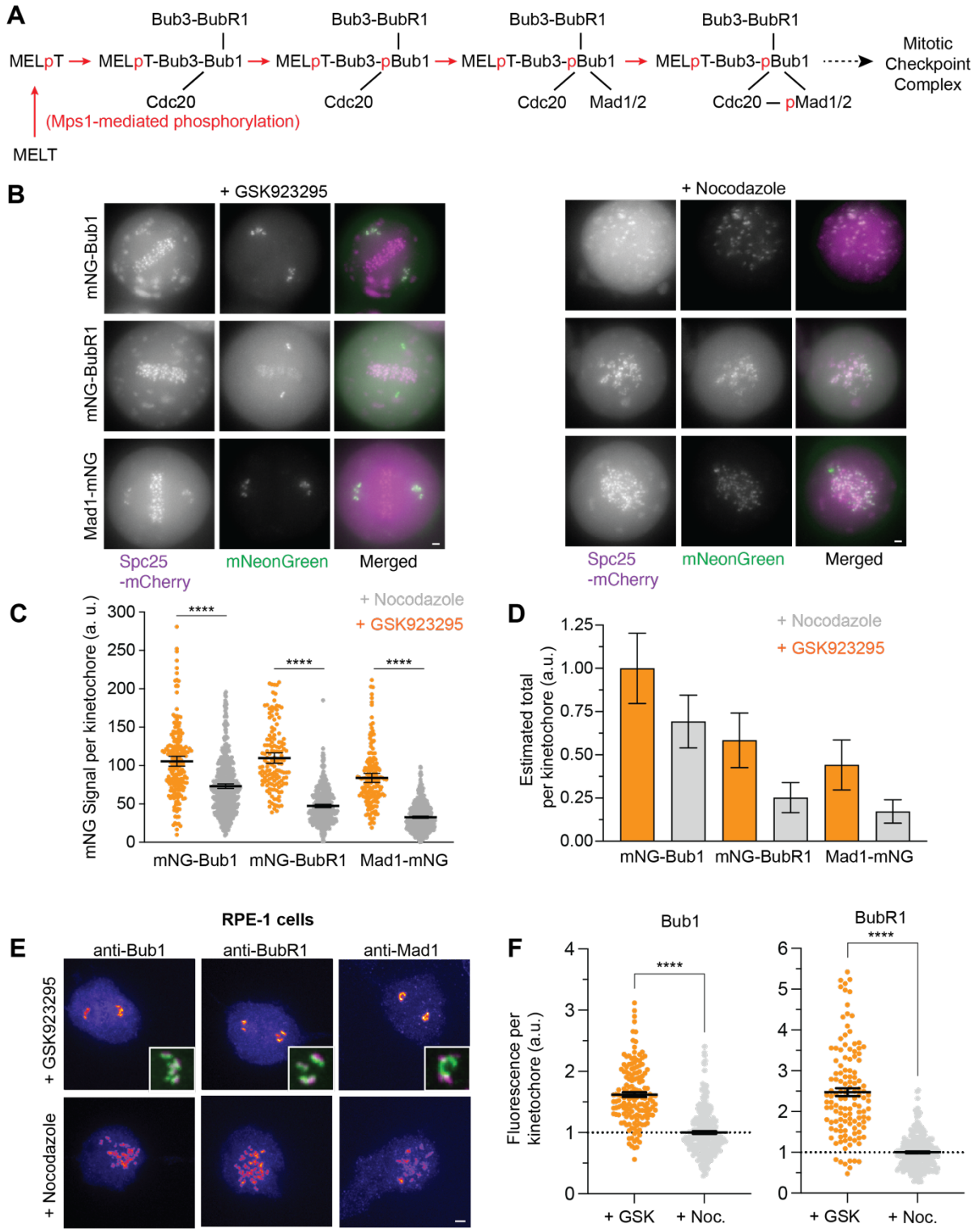

686

687 **Figure 1 The SAC protein recruitment at signaling kinetochores depends on the number of**
688 **signaling kinetochores in the cell.**

689 **(A)** A simplified schematic of the MELT motif-mediated recruitment of SAC proteins to the
690 kinetochore. Red arrows signify Mps1-mediated phosphorylation, black lines indicate protein-
691 protein interactions. The RZZ pathway, which is activated by Bub1 [29,35,40], is not shown.
692 **(B)** Representative fluorescence micrographs of mitotic HeLa cells expressing the indicated
693 proteins treated with GSK923295 (left) and nocodazole (right; scale bar ~ 1.6 μm)
694 **(C)** Quantification of the fluorescence signal per signaling kinetochore. Horizontal lines display
695 mean ± 95% confidence intervals (n = 200, 142, 160 in GSK923295-treated cells and 562, 446,
696 and 658 in nocodazole-treated cells for Bub1, BubR1, and Mad1 respectively, observations
697 pooled from ≥ 2 technical repeats). Right: Spc25-mNG signal per kinetochore quantified from
698 images acquired under identical imaging conditions (n = 178). Welch's *t*-test was used to
699 determine whether the sample means are significantly different. In all the figures in this study, ****
700 indicates $p < 0.0001$, *** indicates $0.0001 < p < 0.001$, ** indicates $0.001 < p < 0.01$, * indicates
701 $0.01 < p < 0.05$, and n.s. (not significant) indicates $p > 0.05$.
702 **(D)** Estimation of total protein recruited per kinetochore based on the fluorescence
703 measurements shown in C and immunoblot quantification of labeled to unlabeled fraction for each
704 protein shown in Figure S1.
705 **(E)** Representative immune-fluorescence micrographs (pseudo-colored as heatmaps) of
706 RPE-1 cells. Insets show magnified regions of interest around unaligned chromosomes with
707 antibodies labeling SAC proteins pseudo colored as green and antibodies labeling centromeres
708 pseudo colored as magenta. Notice in the case of Mad1 a ring-like structure in the polar region
709 presumably representing the Mad1 protein aggregated by its dynein-mediated transport from the
710 kinetochore. This structure prevented us from quantifying the amount of kinetochore localized
711 Mad1. Scale bar ~ 2.44 μm.
712 **(F)** Quantitation of immunofluorescence per kinetochore for Bub1 and BubR1 (each dot
713 represents a single kinetochore; mean ± SEM is overlaid for each group. For Bub1, n = 255
714 (GSK923235-treated) and 157 kinetochores (nocodazole-treated) from two technical repeats. For
715 BubR1, n = 125 (GSK923235-treated) and 288 kinetochores (nocodazole-treated) from two
716 technical repeats. Welch's *t*-test used to compare sample means.

717

718

719

720

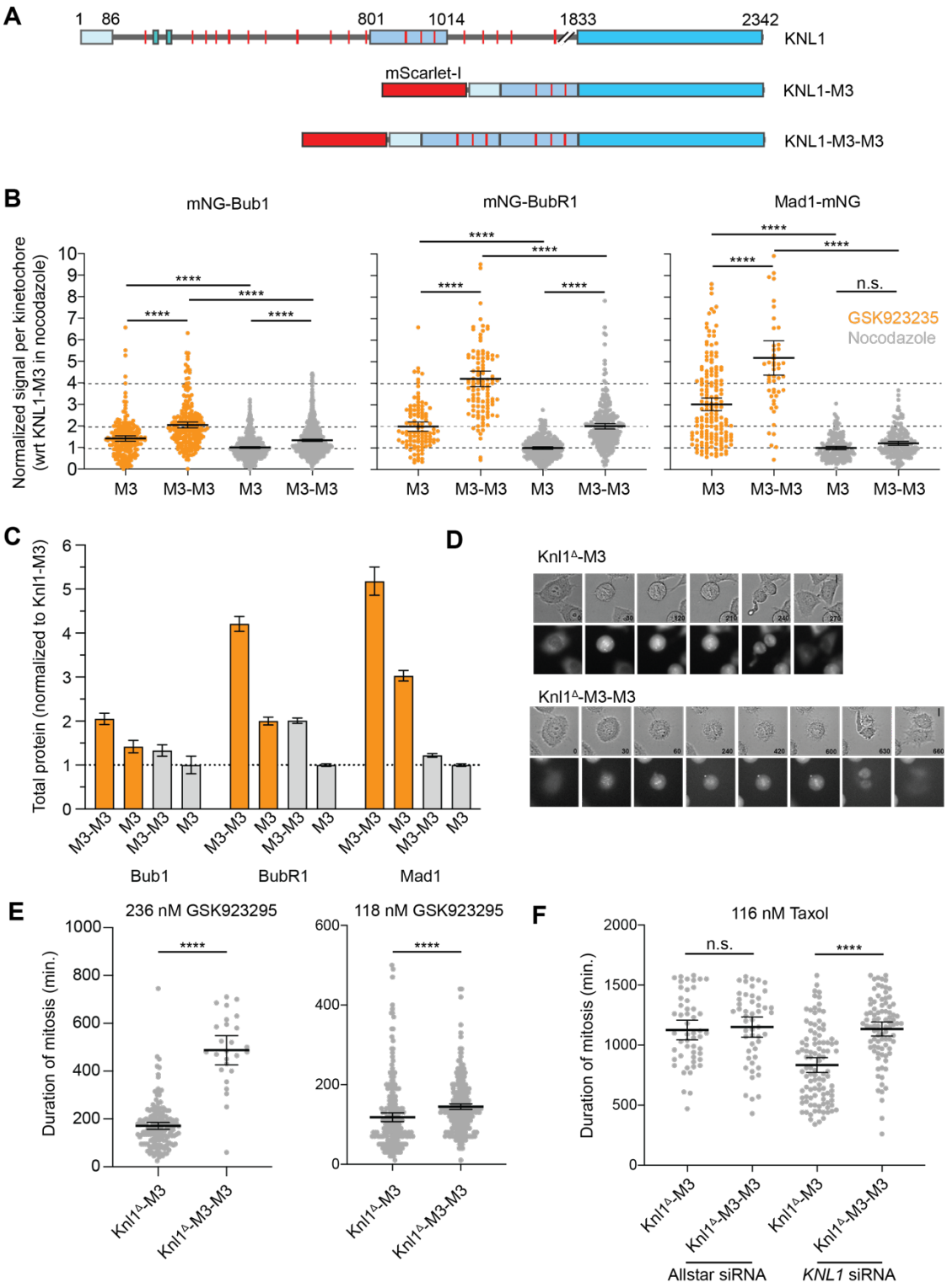

721
722 **Figure 2 The number of MELT motifs in Knl1 affects SAC protein recruitment to the**
723 **kinetochore and SAC signaling strength.**

724 **(A)** Schematics of the full-length, endogenous Knl1 and the recombinant Knl1$^{\Delta}$-M3 and Knl1$^{\Delta}$-
725 M3-M3 versions. The expression of Knl1$^{\Delta}$-M3 (or Knl1$^{\Delta}$-M3-M3) is under the regulation of a
726 constitutive *EF1a* promoter.
727 **(B)** Quantification of the fluorescence signal per signaling kinetochore for the indicated
728 protein. In each case, the signals were normalized using the mean signal for each protein
729 measured in nocodazole-treated cells expressing Knl1$^{\Delta}$-M3 (mNG-Bub1: n =844 and 602 for
730 Knl1$^{\Delta}$-M3-M3 and Knl1$^{\Delta}$-M3 respectively in nocodazole-treated cells and 222 and 120 for Knl1$^{\Delta}$-
731 M3-M3 and Knl1$^{\Delta}$-M3 respectively in GSK923295-treated cells, pooled from ≥ 2 technical repeats;
732 mNG-BubR1: n = 278 and 272 for Knl1$^{\Delta}$-M3-M3 and Knl1$^{\Delta}$-M3 respectively in nocodazole-treated
733 cells and 110 and 107 for Knl1$^{\Delta}$-M3-M3 and Knl1$^{\Delta}$-M3 respectively in GSK923295-treated cells,
734 pooled from ≥ 2 technical repeats; Mad1-mNG: n = 182 and 184 for Knl1$^{\Delta}$-M3-M3 and Knl1$^{\Delta}$-M3
735 respectively in nocodazole-treated cells and 52 and 166 for Knl1$^{\Delta}$-M3-M3 and Knl1$^{\Delta}$-M3
736 respectively in GSK923295-treated cells, pooled from ≥ 2 technical repeats).
737 **(C)** Estimation of total protein amount per kinetochore relative to the total Bub1 amount per
738 kinetochore in drug-treated cells (colors same as in as in B).
739 **(D)** Representative micrographs show mitotic progression of cells with either Knl1$^{\Delta}$-M3 (top)
740 or Knl1$^{\Delta}$-M3-M3 (bottom, scale bar: 10 μm). Time stamps are in minutes.

741 **(E-F)** Duration of mitosis for cells treated with the indicated concentration of GSK923295 and
742 Taxol (left: n = 162 and 26 for Knl1$^{\Delta}$-M3 and Knl1$^{\Delta}$-M3-M3 respectively from two technical repeats;
743 right: n = 235 and 339 for Knl1$^{\Delta}$-M3 and Knl1$^{\Delta}$-M3-M3 respectively, n = 51 and 52 for Allstar siRNA
744 + taxol treatment and n = 102 and 88 for KNL1 siRNA + taxol treatment for Knl1$^{\Delta}$-M3 and Knl1$^{\Delta}$-
745 M3-M3 respectively). Welch's *t*-test was used to compare sample means.

746
747
748
749
750
751
752
753

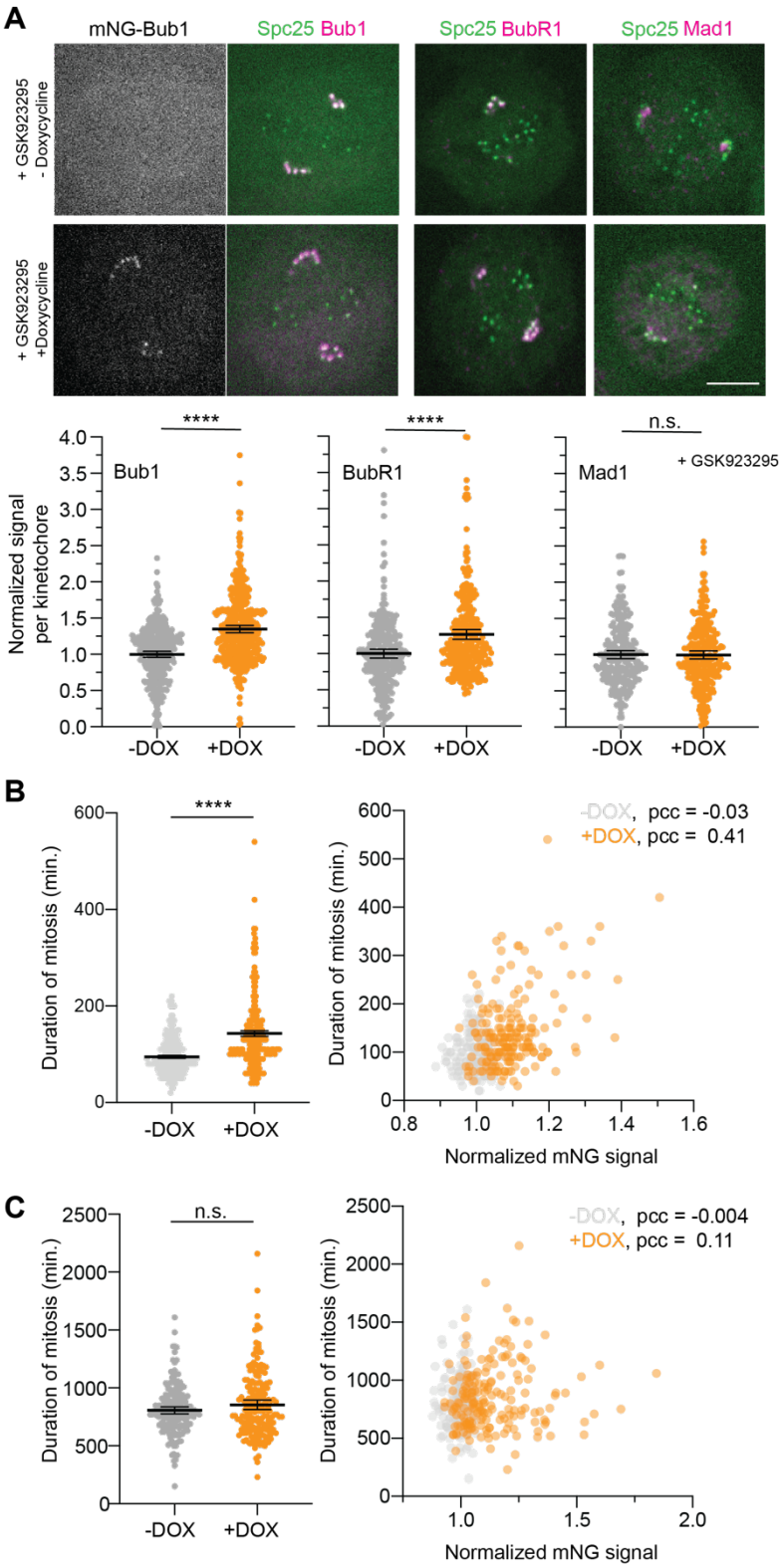

Figure 3 – Bub1 over-expression results in higher Bub1 and BubR1 recruitment per kinetochore and prolongs the delay in anaphase onset.

757 **(A)** Top panel: representative fluorescence micrographs of control (top) cells and cells treated
758 with doxycycline to exogenously express mNG-Bub1. Scale bar ~ 4.92 μm. Bottom panel:
759 quantification of immunofluorescence signal per kinetochore for the indicated proteins in control
760 cells and cells treated with doxycycline to induce exogenous mNG-Bub1 expression. Signal
761 values were normalized with the average signal for the respective protein in doxycycline-untreated
762 cells. (n = 344 and 390 for Bub1, 346 and 387 for BubR1, and 234 and 275 for Mad1 in untreated
763 and doxycycline-treated cells respectively, observations pooled from 3 technical repeats).
764 Welch's *t*-test used to compare sample means.
765 **(B)** Left: Duration of mitosis in control and doxycycline-treated cells in media containing 25-
766 37 nM GSK923295 (n = 195 and 187 for untreated and doxycycline-treated cells respectively,
767 from 2 technical repeats; $p < 0.0001$ for doxycycline-treated and GSK923295 treated cells).
768 Horizontal lines represent mean ± 95% confidence intervals on the mean. Right: Correlation
769 between the duration of mitosis and the average cellular level of the exogenously expressed
770 mNG-Bub1. mNG-Bub1 signal per cell was normalized with the average signal measured in
771 control cells. Pearson's correlation coefficient (pcc) for each data set is noted in the figure (p =
772 0.6222 and < 0.0001 respectively for untreated and doxycycline-treated cells respectively)
773 **(C)** Left: Duration of mitosis in control and doxycycline-treated cells in media containing 330
774 nM nocodazole (n = 189 and 185 for untreated and doxycycline-treated cells respectively, from 2
775 technical repeats). Horizontal lines represent mean ± 95% confidence intervals on the mean.
776 Right: Correlation between the duration of mitosis and the average cellular level of the
777 exogenously expressed mNG-Bub1. mNG-Bub1 signal per cell was normalized with the average
778 signal measured in control cells. Pearson's correlation coefficient (pcc) for each data set is noted
779 in the figure (p = 0.053 and 0.1309 respectively for untreated and doxycycline-treated cells
780 respectively).

781

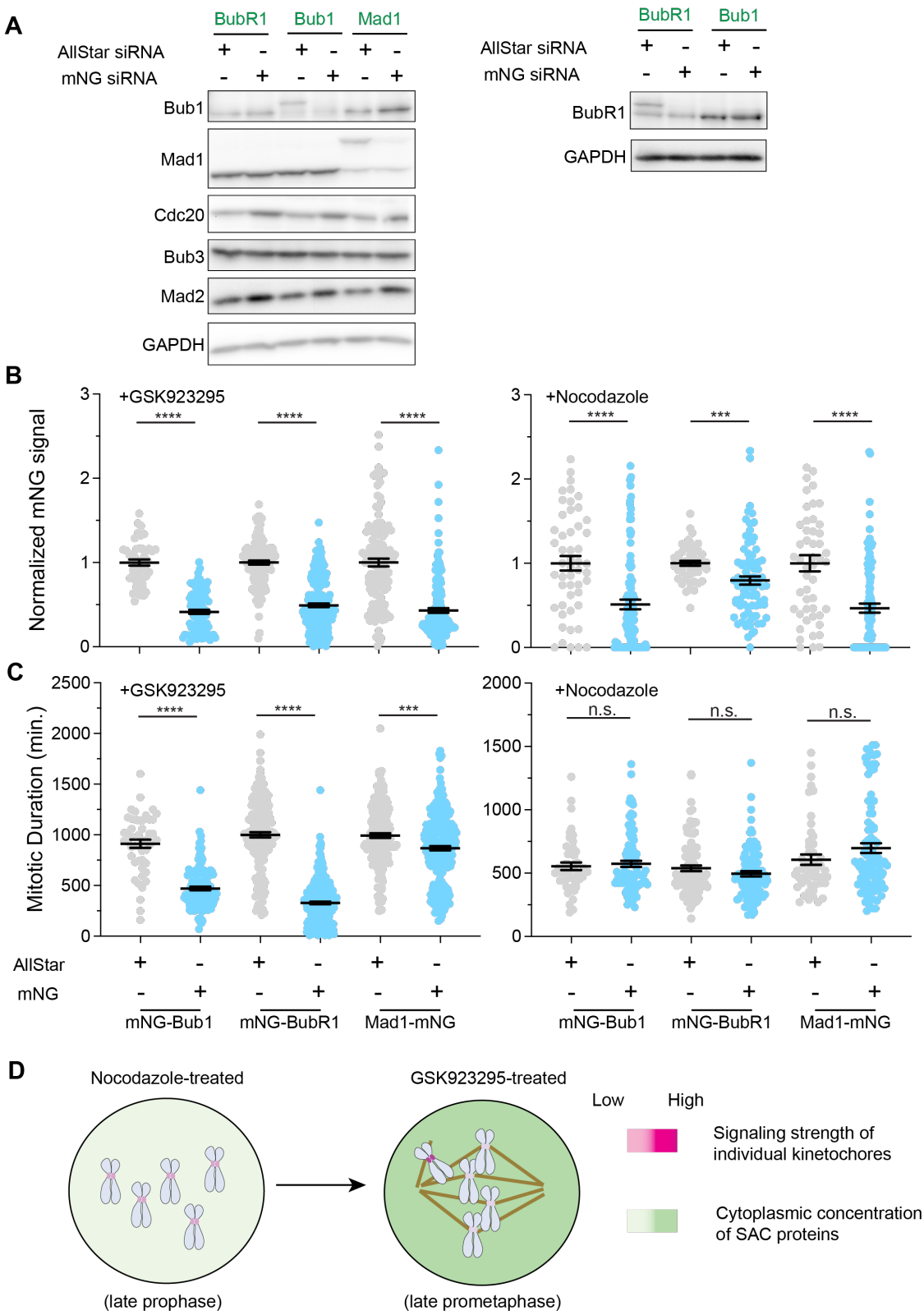
A
BubR1
Bub1
Mad1
AllStar siRNA
mNG siRNA
Bub1
Mad1
Cdc20
Bub3
Mad2
GAPDH
BubR1
Bub1
AllStar siRNA
mNG siRNA
BubR1
GAPDH
B
+GSK923295
+Nocodazole
Normalized mNG signal
C
+GSK923295
+Nocodazole
Mitotic Duration (min.)
n.s.
AllStar
mNG
mNG-Bub1
mNG-BubR1
Mad1-mNG
D
Nocodazole-treated
GSK923295-treated
Low
High
Signaling strength of individual kinetochores
Cytoplasmic concentration of SAC proteins
(late prophase)
(late prometaphase)

782

783 **Figure 4 – Partial depletion of Bub1 and BubR1, but not Mad1, weakens the signaling**
784 **potential of the SAC.**

785 **(A)** Immunoblot analysis of total cell lysates shows that the mNG-tagged SAC protein is
786 specifically targeted for RNAi after a 48-hour treatment with mNG siRNA.
787 **(B)** Quantification of the mNG-signal per cell under the indicated conditions (For the
788 experiment involving GSK923295 treatment, n = 50, 126, 130 for mNG-Bub1, mNG-BubR1, and
789 Mad1-mNG cells respectively treated with Allstar siRNA; n = 100, 219, and 177 for mNG-Bub1,
790 mNG-BubR1, and Mad1-mNG cells respectively treated with mNG siRNA; data collected in two
791 technical repeats). For the experiment involving nocodazole treatment, n = 50, 50, and 50 for
792 mNG-Bub1, mNG-BubR1, and Mad1-mNG cells respectively treated with Allstar siRNA; n = 100,
793 85, and 100 for mNG-Bub1, mNG-BubR1, and Mad1-mNG cells respectively treated with mNG
794 siRNA; data collected from 2 technical repeats). Each dot represents a measurement from one
795 cell, mean ± SEM overlaid. Welch's *t*-test used to compare sample means.
796 **(C)** Duration of mitosis for same cells as in B in media containing GSK923295 and nocodazole
797 (for GSK923295-treated cells: $p \leq 0.0001$ based on ordinary one-way ANOVA; for nocodazole-
798 treated cells, $p > 0.253$ based on ordinary one-way ANOVA). Each dot represents a measurement
799 from one cell, mean ± SEM overlaid. Pairwise comparisons of sample means performed using
800 Tukey's multiple comparison test.
801 **(D)** Model depicts the combined effect of the number of signaling kinetochores per cell and
802 the availability of free, cytoplasmic SAC proteins on the signaling strength of individual
803 kinetochores.

804
805

806

807 **Supplementary figures**

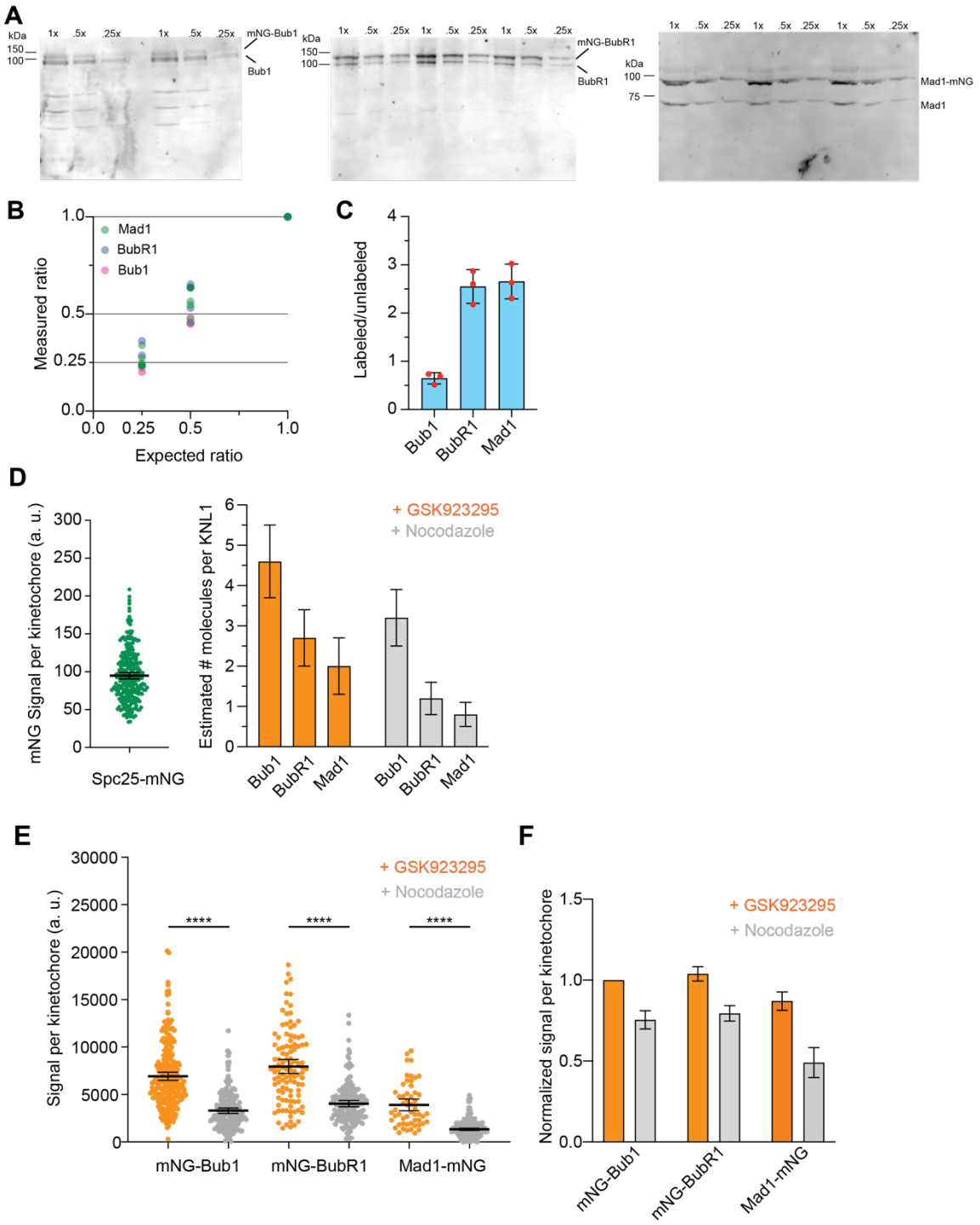

808

809 **Figure S1 (related to Figure 1) Assessment of the relative amounts of mNG-labeled and**
810 **unlabeled proteins in the three cell lines.**

811 **(A)** Immunoblot analysis of whole mitotic cell lysates of the three cell lines probing for the
812 indicated proteins. Two out of the three technical repeats for the mNG-Bub1 cell line and all three
813 technical repeats for the mNG-BubR1 and Mad1-mNG cell lines are displayed. Numbers at the
814 top denote the lysate volume loaded to ascertain the linearity of the fluorescent secondary
815 antibody signal.
816 **(B)** Ratio metric analysis of serial dilutions confirms that band intensities are directly
817 proportional to the amount of protein loaded. The band intensities were quantified using the 'Gel
818 Analyzer' tool in Fiji. The ratio of labeled to unlabeled protein for each technical repeat was defined
819 as the average of the ratios for the three 'repeats'.
820 (C) The ratio of the mNG-tagged to unlabeled species for the three proteins. Error bars display
821 the standard deviation.
822 (D) Left: the beeswarm plot displays the quantification of Spc25-mNG signal per kinetochore
823 in images obtained under identical imaging conditions as in Figure 1C. The bar plot on the right
824 displays the estimated number of molecules of the mNG-tagged SAC protein per Knl1 calculated
825 by dividing the mean signal per kinetochore for each protein with the mean Spc25-mNG signal
826 per kinetochore as the reference. Error bars represent mean ± SEM.

827 **(E)** Left: Quantification of the fluorescence signal per signaling kinetochore in cells treated with
828 siRNA against *ZW10* (n = 108, 242, 54 in GSK923295-treated cells and 166, 178, 219 in
829 nocodazole-treated cells for Bub1, BubR1, and Mad1, respectively, pooled from 2 technical
830 repeats).

831 **(F)** Average signals from E are normalized using the mNG-Bub1 signal per kinetochore.
832 Horizontal lines display the standard error on the mean ratio.

833

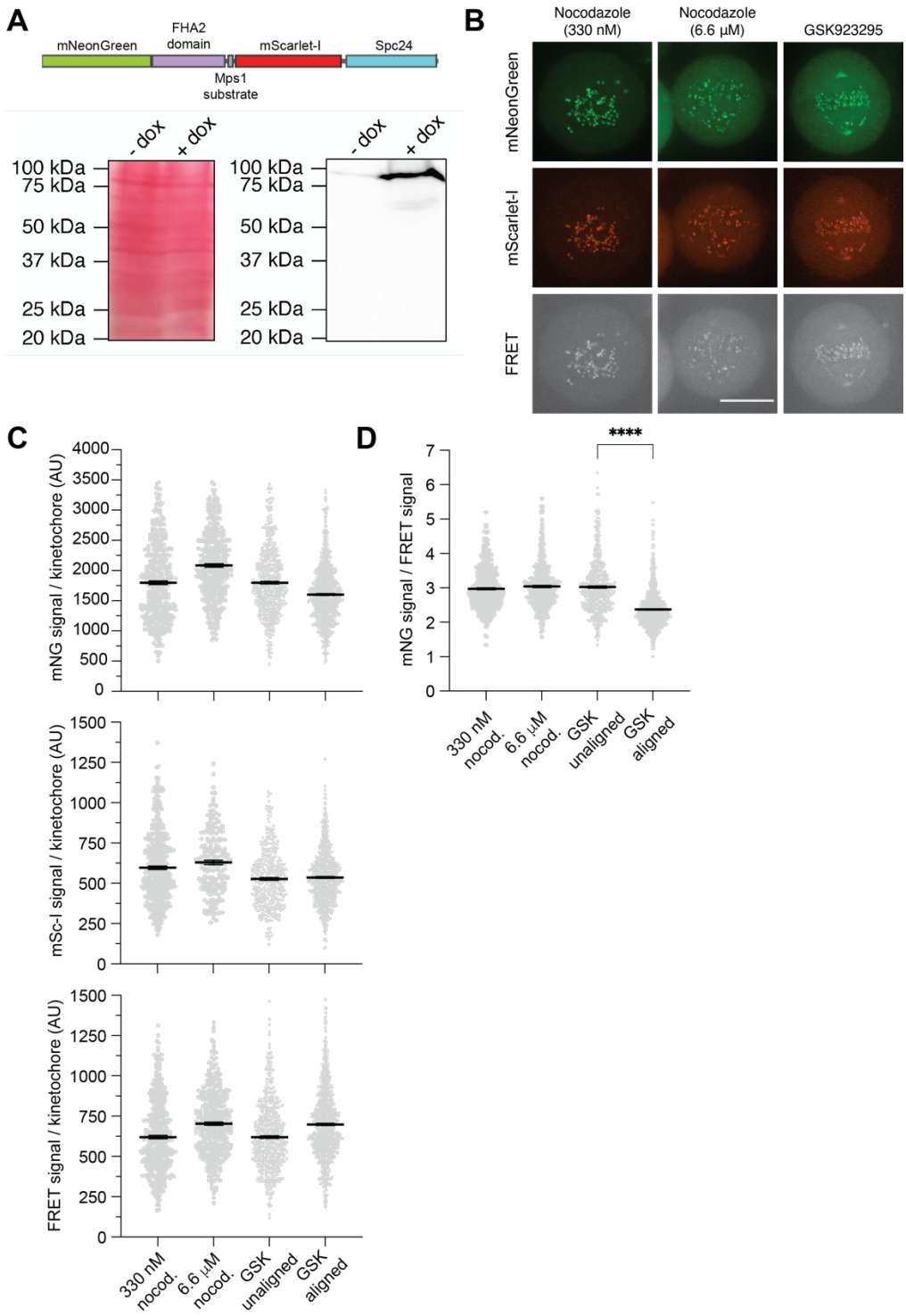

834

835 **Supplementary Figure S2 (related to Figure 1) Net phosphorylation at signaling**
836 **kinetochores is the same in nocodazole- and GSK923295-treated cells.**

837 **(A)** Top: Schematic of the modified MPS1sen-KT [34] that uses the mNeonGreen and mScarlet-I
838 as the FRET pair. Bottom: Using an antibody against DsRed2 (which detects mScarlet-I), we

839 confirmed that MPS1sen-KT (with a theoretical molecular weight of 97.2 kDa) is expressed as a
840 full-length protein with negligible partial degradation in HeLa A12 treated with doxycycline. A
841 Ponceau S staining of the same blot before membrane blocking (left panel) serves as the loading
842 and membrane transferring control.
843 **(B)** Representative images of cells expressing MPS1sen-KT. The look-up table for each channel
844 (row) is universal for different groups (column). Scale bar, 10 μm.
845 **(C)** Raw fluorescence quantification at signaling kinetochores under various drug treatments in
846 the green, red, and FRET channels. Each gray dot represents a single kinetochore measurement.
847 Data from cells treated with 45 nM, 90 nM, and 200 nM GSK923295 were pooled together (the
848 mean values are not significantly different from one another; data not shown) to simplify the
849 presentation. Data were compiled from at least two independent experiments (more than 40 cells
850 in total for each group). Mean values ± 95% confidence intervals are overlaid. The variation across
851 different groups can be attributed to different FRET efficiencies (which we intend to quantify) and
852 day-to-day variations in the doxycycline-induced expression of MPS1sen-KT. To cancel the effect
853 of these variations, a normalized metric of the FRET efficiency (mNG/FRET) was used in this
854 study.

855 **(D)** A summary of a normalized FRET metric (mNeonGreen signal/FRET signal) in HeLa A12
856 cells treated with different drugs at various concentrations. Each gray dot represents a single
857 kinetochore measurement. Data were compiled from at least two independent experiments (more
858 than 40 cells in total for each group). As in C, Data from cells treated with 45 nM, 90 nM, and 200
859 nM GSK923295 were pooled together. Mean values ± 95% confidence intervals are overlaid. The
860 Welch's ANOVA test [W(DFn,DFd) = 1 .339(2.000,917.0), P = 0.2626] was performed for the first
861 3 columns (unaligned, signaling kinetochores). The unpaired t-test with Welch's correction
862 (P<0.0001) was performed to compare aligned non-signaling kinetochores with unaligned
863 signaling kinetochores in GSK923295-treated cells.
864
865
866

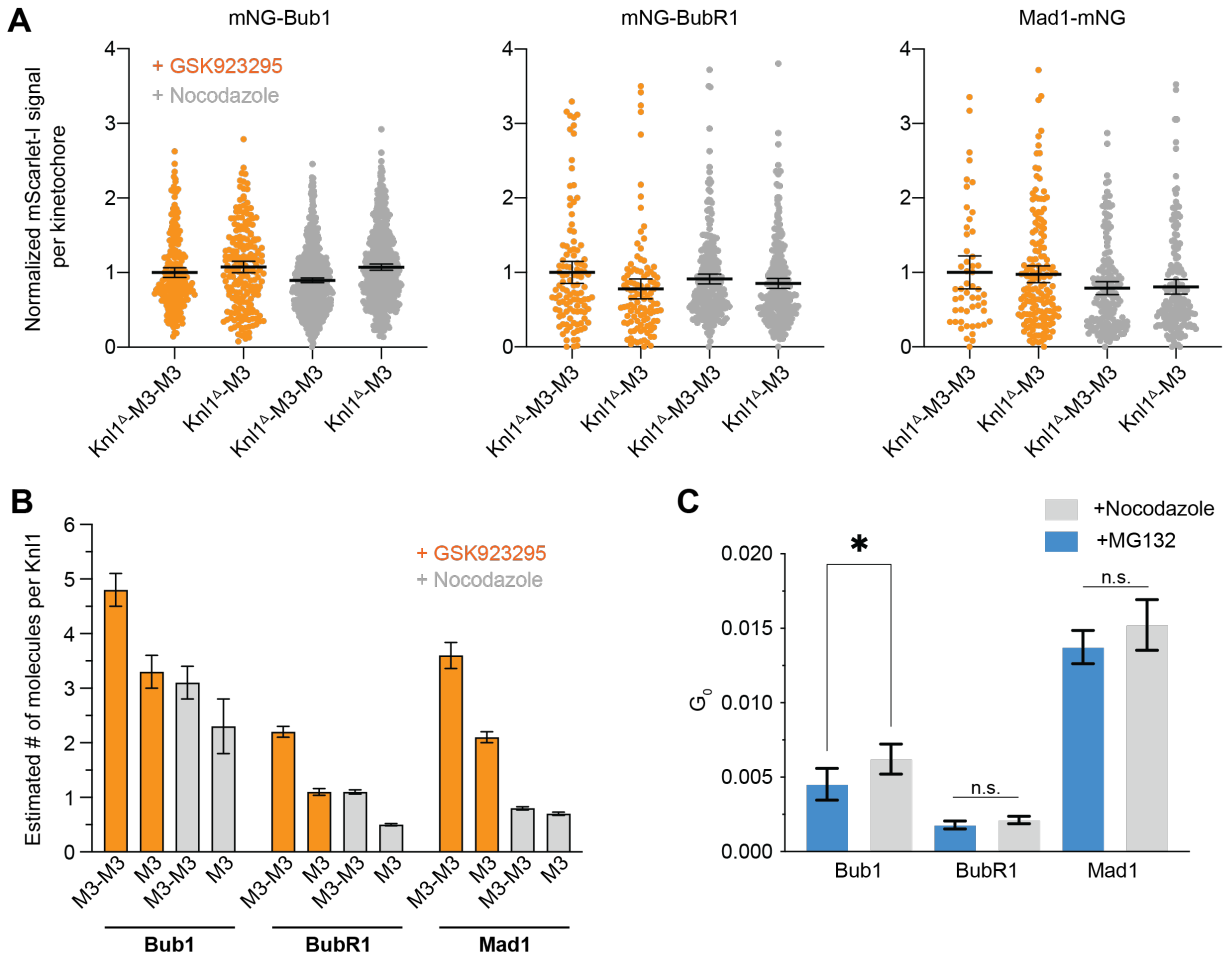

867

868 **Figure S3 (related to Figure 2) Assessment of the kinetochore recruitment of mScarlet-I-**
869 **Knl1$^{\Delta}$-M3-M3 and mScarlet-I-Knl1$^{\Delta}$-M3**.

870 **(A)** mScarlet-I fluorescence signal per kinetochore indicating the amount of recombinant Knl1
871 versions (noted by the X-axis labels). Minor differences in the incorporation of the recombinant
872 Knl1 cannot explain the observed differences in SAC protein recruitment in each case. Note that
873 the average value for the mScarlet-I-Knl1$^{\Delta}$-M3-M3 signal in GSK939295 in each data set was
874 used as the normalization factor for each cell line. The numbers of data points are identical to
875 those in Figure 2.

876 **(B)** Estimation of the copy number of each SAC protein per Knl1 molecule using the Spc25-mNG
877 fluorescence signal per kinetochore as the fiduciary standard (shown in Figure S1). Error bars
878 indicate mean ± SEM.

879 **(C)** G_0 of the three proteins in metaphase-arrested (MG-132-treated) and nocodazole-treated
880 cells as measured by Fluorescence Correlation Spectroscopy (FCS). This is the magnitude of the

881 auto-correlation function for the fluorescence fluctuation data for 0-time delay. It is inversely
882 proportional to the average number of fluorophores in the focal volume, i.e. the concentration of
883 the fluorophore [57]. Mean values under the two conditions compared using Welch's *t*-test.

884

885

886

887

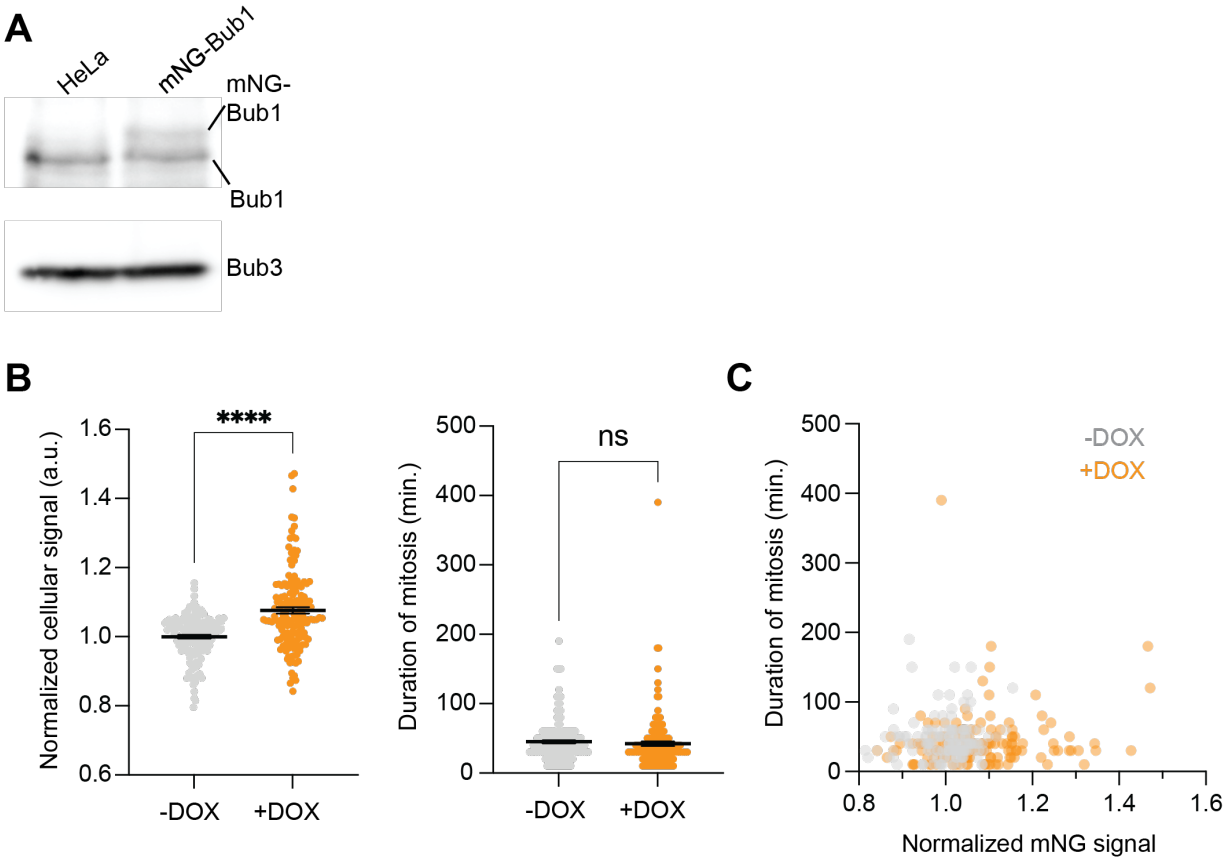

Figure S4 (related to Figure 3) mNG-Bub1 over-expression does not affect normal mitotic progression of HeLa A12 cells.

(A) Immunoblot shows doxycycline-induced expression of exogenous mNG-Bub1.

(B) Left: The average mNG signal in mitotic HeLa cells that are either untreated or treated with doxycycline to induce exogenous mNG-Bub1 expression (normalized to the average value of mNG fluorescence in untreated cells, which also represents the background signal). Right: the duration of mitosis for the same cells. (n = 155 and 154 for -dox and +dox respectively pooled from 2 technical repeats). The horizontal lines indicate mean ± SEM. Welch's *t*-test was used to compare the sample means.

(C) Scatterplot displays the correlation between the cellular mNG signal (normalized as in B) and the duration of mitosis (Pearson's correlation coefficient = 0.05 and 0.13 with p = 0.5 and 0.1 for -Dox and +Dox respectively).

901 **Supplementary Videos**

902 **Video S1 –** Time-lapse imaging of HeLa cells treated with 25 nM GSK923295. Time - hr:min.

903 **Video S2 -** Time-lapse imaging of HeLa cells treated with 25 nM GSK923295 and 1 µg/ml of
904 Doxycycline to exogenously over-express mNG-Bub1. Time - hr:min.

905 **Video S3** - Time-lapse imaging of HeLa cells treated with 330 nM Nocodazole. Time - hr:min.

906 **Video S4 -** Time-lapse imaging of HeLa cells treated with 330 nM Nocodazole and 1 µg/ml of
907 Doxycycline to exogenously over-express mNG-Bub1. Time - hr:min.

908 **Video S5 –** Time-lapse imaging of genome-edited HeLa cells heterozygous for mNG-Bub1 and
909 exogenously expressing H2B-mCherry. Cells were released from a G1/S block into media
910 containing 236 nM GSK923295. Time - hr:min.

911 **Video S6 –** Time-lapse imaging of genome-edited HeLa cells heterozygous for mNG-Bub1 and
912 exogenously expressing H2B-mCherry. Cells were treated with siRNA targeting mNG to partially
913 deplete BubR1 and released from a G1/S block into media containing 236 nM GSK923295. Time
914 - hr:min.